A PILOT SCALE DESIGN OF ASH DEPOSITION MEASUREMENT ON SUPERHEATER TUBE FOR INDUSTRIAL BOILER

NICHA KHIMLAP

YUTTAKANT VARISREE

A THESIS SUBMITTED IN PARTIAL FULFILMENT

OF REQUIREMENTS FOR THE DEGREE OF

BACHELOR OF ENGINEERING IN MECHANICAL ENGINEERING

FACULTY OF ENGINEERING

SCHOOL OF INTERNATIONAL DISCIPLINARY ENGINEERING PROGRAMS

KING MONGKUT'S INSTITUTE OF TECHNONOGY LADKRABANG

ACADEMIC YEAR 2022

THESIS PROJECT OF YEAR 2022

MECHANICAL ENGINEERING FACULTY OF ENGINEER

KING MONGKUT'S INSTITUTE OF TECHNONOGY LADKRABANG

Project Title A Pilot Scale Design of Ash Deposition Measurement on Superheater Tube for Industrial Boiler

Student Name

1. Nicha Khimlap Student ID 62011168
2. Yuttakant Varisree Student ID 62011298

Ponepen Laphirattanakul Advisor

(Asst.Prof.Dr. Ponepen Laphirattanakul)

A Pilot Scale Design of Ash Deposition Measurement on Superheater Tube for Industrial Boiler

Nicha Khimlap Student ID 62011168
Yuttakant Varisree Student ID 62011298
Advisor Asst.Prof.Dr. Ponepen Laphirattanakul
Academic year 2022

Abstract

The purpose of this project was to study the physical and chemical phenomena that cause the deposition on superheater in a water tube boiler and design the pilot scale for ash deposition measurement. The scope includes the calculation of heat transfer mode of the superheater tubes, which are conduction and convection in crossflow pattern, and the superheater tubes parameters e.g., diameter, area. These were aimed to enhance the mass flow rate of working fluid used in pilot scale that could mimic the deposition mechanism on superheated tube. Actual data was obtained based on a YOSHIMINE water-tube boiler with 80 ton/hr of capacity. Based on the limit and boundary encountered, the test kit properties are calculated, and the system components are selected. Finally, a 3D pilot scale design for measuring ash deposition on superheater tube is successfully developed.

Keywords: Superheater tubes, Ash deposition, Fouling, Slagging, Biomass fuel

Acknowledgement

This thesis is completed due to the direction, expertise, and the sharing of priceless experiences from Asst.Prof.Dr Ponepen Laphirattanakul, who is the assistant professor of our project. Without them, we would be unable to effectively complete our project thesis entitled "A Pilot Scale Design of Ash Deposition Measurement on Superheater Tube for Industrial Boiler." We would like to express our deepest admiration and appreciation to the professors, friends, and seniors who helped us along this road.

Finally, we would like to thank King Mongkut's Institute of Technology Ladkrabang, which provided support and resources for this project, including information and access to research papers.

Nicha Khimlap

Yuttakant Varisree

Table of Contents

Abstract ii

Acknowledgement iii

List of Figures vii

List of Tables x

Abbreviation and Symbols xi

CHAPTER 1 1

1.1 Background 1

1.2 Objectives 2

1.3 Hypotheses 2

1.4 Project Scopes 2

1.5 Procedures 3

1.6 Expected Outcomes 3

CHAPTER 2 4

CHAPTER 3 13

3.1 Boiler 13

3.1.1 Boiler type 13

3.1.2 Thermodynamics in boiler 16

3.1.3 Boiler efficiency 18

3.2 Combustion of biomass 19

3.2.1 Solid fuel combustion 19

3.2.2 Biomass fuel combustion 20

3.3 Ash composition, formation, and deposition 21
3.3.1 Ash composition 21
3.3.2 Ash formation 23
3.3.3 Ash deposition mechanisms 24
3.4 Slagging, fouling, and their effects 29
3.5 Heat transfer [7] 30
3.5.1 Conduction 30
3.5.2 Convection 31
3.5.3 Overall heat transfer coefficient (U) 32
3.6 Pressure Loss and Head Loss [13] 34
3.7 Pump [13] 38
3.7.1 Type of pump [14] 38
3.8 Radiator [15] 39
CHAPTER 4 44
4.1 Heat flux of superheater calculation 47
4.2 Test kit calculation 49
CHAPTER 5 55
5.1 Test kit 57
5.1.1 Ash deposit accumulator tube 58
5.1.2 Pump 59
5.1.3 Radiator 61
5.1.4 Water tank 62
CHAPTER 6 64

6.1 Conclusion 64

6.2 Recommendations 65

6.3 Further study 66

References 72

List of Figures

Figure 1.1 Superheater tubes in a coal fired boiler. 2
Figure 2.1 The appearance of the deposit 7
Figure 2.3 The relative heat uptake, deposit mass, fouling resistance in the function of time of low-temp experiment. 8
Figure 2.4 The relative heat uptake, deposit mass, fouling resistance in the function of time of high-temp experiment 9
Figure 2.5 The composition of different position of ash of low temperature combustion 10
Figure 2.6 The composition of different position of ash of high temperature combustion 10
Figure 2.7 Samples of ash deposition on pipe 12
Figure 3.1 Water tube boiler diagram 13
Figure 3.2 Water tube boiler 14
Figure 3.3 Fire tube boiler 14
Figure 3.4 Fire tube boiler 15
Figure 3.5 Hybrid boiler 15
Figure 3.6 T-H Diagram of water to steam (converting water into superheated steam) 17
Figure 3.7 Solid Fuel Combustion 20
Figure 3.8 Ash formation from solid fuel combustion 24
Figure 3.9 Inertial impaction 26
Figure 3.10 Impaction efficiency which equals to mass of impacting particle over the total flowing mass 26
Figure 3.11 Thermophoretic force acting on particles in thermal boundary layer of heat exchanger surface 27
Figure 3.12 Ash was deposited by the transport mechanism on the heat exchanger surface. 28

Figure 3.13 The equivalent roughness values for new commercial pipes. 35
Figure 3.14 Loss coefficient K_L of various pipe components for turbulent flow. 36
Figure 3.15 Loss coefficient K_L of various pipe components for turbulent flow. 37
Figure 3.16 A common centrifugal pump from the side view and front view. 38
Figure 3.17 Two basic styles of radiator 40
Figure 3.18 The effectiveness of cross flow heat exchanger such as radiator can be obtained. 43
Figure 4.1 Process Flowchart 46
Figure 4.2 Heat flux calculation 47
Figure 4.3 The heat transfer area can be obtained by the information from the factory. 49
Figure 4.4 The graph of shows the different working fluids. 50
Figure 4.5 The graph can be plotted by vary the pipe length in accordance with the STBA 22 JIS G3462-1988 standard. 52
Figure 5.1 The test kit location on real plant. 55
Figure 5.2 The test kit design 57
Figure 5.3 The ash deposit accumulator tube 58
Figure 5.4 The characteristic curve of selected pump. 59
Figure 5.5 Pump dimension 60
Figure 5.6 The pump design on the test kit 60
Figure 5.7 Schematic of designed radiator 61
Figure 5.8 The radiator designed on the test kit. 61
Figure 5.9 The tank design on the test kit. 62
Figure 6.1 Components of Heat flow meter. 68
Figure 6.2 HANI Clamp-on Temperature Sensor 68
Figure 6.3 Thermocouple Type-K 69
Figure 6.4 Type K Single Input Thermometer 69
Figure 6.5 Siemens Electromagnetic flowmeters 70

Figure 6.6 Transmitter for flowmeters 71
Figure 6.7 Pressure Gauge 71

List of Tables

Table 2.1 The selected study dealing with ash deposition mechanism, composition 4
Table 2.2 The experiment condition T. Madhiyanon et al. 8
Table 3.1 The ash compositions of different kinds of biomass 22
Table 3.2 The properties of biomass fuel 22
Table 3.3 The fouling factor of different fluid 33
Table 4.1 The properties of saturated vapor and superheat steam 48
Table 4.2 The comparison of the value each working fluid yields..... 49
Table 4.3 The parameter used in calculating the pressure loss. 52
Table 4.4 Alloy Steel Boiler and Heat Exchanger Tubes – STBA 53
Table 4.5 Carbon Steel – Alloy Steel, Pipe and Tube 54
Table 5.1 The operating condition of test kit..... 56
Table 5.2 Property of selected radiator..... 62

Abbreviation and Symbols

Re_p	Particle Reynold number, $(-)$
ρ_g	Density of particle, (kg/m^3)
μ_g	Viscosity of particle, $(\frac{kg}{m \cdot s})$
u_p	average velocity of particle, (m/s)
d_p	particle diameter, (m)
d_c	Pipe or tube diameter, (m)
E	Energy, (kJ)
H	Enthalpy, (kJ)
m	Mass, (kg)
$\dot{m}$	Mass flow rate, (kg/s)
v	Velocity, (m/s)
g	Gravitational acceleration, (m/s^2)
z	Height, (m)
W	Work, (kJ)
m_f	Mass of fuel, (kg)
HV	Heating value, $(\frac{kJ}{kg})$
m_w	Mass of water, (kg)
h_{steam}	Enthalpy of steam, $(\frac{kJ}{kg})$

h_{fw}	Enthalpy of feed water, $(\frac{kJ}{kg})$
HHV	Higher heating value, $(\frac{kJ}{kg})$
LHV	Lower heating value, $(\frac{kJ}{kg})$
h_{fg}	Enthalpy of vaporization, $(\frac{kJ}{kg})$
η_{th}	Thermal efficiency, $(-)$
St^c	Correction Stoke number, $(-)$
ψ	Correction factor, $(-)$
F_T	Action force cause by thermophoresis, (N)
∇T_g	Temperature gradient, $(\frac{K}{m}, \frac{C^o}{m})$
Re	Reynold number, $(-)$
D	Pipe or tube diameter, (m)
G_i	Capture efficiency of particle, $(-)$
T_i	Deposition rate cause by thermophoresis $(kg/s, g/s)$
R_i	Chemical reaction rate $(kg/s, g/s)$
I_i	impaction rate of inertia force. $(kg/s, g/s)$
$\dot{Q}$	Heat transfer rate, $(\frac{J}{s}, W)$
k	Thermal conductivity, $(\frac{W}{m \cdot K})$
A	Heat transfer area, (m^2)

ΔT	Temperature difference, (C^o)
L	Length, (m)
h	Convection heat transfer coefficient, $(\frac{W}{m^2 \cdot K})$
A_c	Cross-section area, (m^2)
$\dot{V}$	Volumetric flowrate, $(\frac{m^3}{s})$
A_s	Surface area, (m^2)
T_s	Surface temperature, (K)
T_∞	Fluid temperature, (K)
R	Thermal resistance, $(\frac{W}{m \cdot K})$
U	Overall heat transfer coefficient, $(\frac{K}{W}, \frac{C^o}{W})$
R_f	Fouling factor, $(m^2 \cdot \frac{K}{W})$
ΔT_{lm}	Log-mean temperature difference, (C^o)
ε	Emissivity, $(-)$
σ	Stefan-Boltzmann constant, $(\frac{W}{m^2 \cdot K^4})$
m_v	Devolatilization mass, (kg)
t	Time, (s)
E_A	Activation energy (kJ / mol)
A_v	Factor exponential of devolatilization, (s^{-1})
k	Reactivity, (s^{-1})

R_u	Universal gas constant, $(\frac{J}{K \cdot mol})$
XRF	X-ray fluorescence
SEM/EDX	Scanning Electron Microscopy (SEM) with Energy Dispersive X-Ray
γ	Specific weight, $(\frac{N}{m^3})$
f	Friction factor, (-)
K_L	Minor loss coefficient, (-)
ΔP	Pressure drops, (Pa)
ε	Material roughness, (mm)
Re	Reynold number, $(-)$
μ	Dynamic viscosity, $(\frac{kg}{m \cdot s})$
ν	Kinematic viscosity, $(\frac{kg}{m \cdot s})$
c_p	Specific heat, $(\frac{kJ}{kg \cdot K})$
Nu	Nusselt number, $(-)$
NTU	Number of transfer units, $(-)$
P	Perimeter, (m)
D_h	Hydraulic diameter, (m)

CHAPTER 1
INTRODUCTION

1.1 Background

Over the course of the 20th century, the human population increased from 1.6 billion to 6.1 billion. During this period, CO_2 emissions, the primary greenhouse gas, increased twelvefold. And with the global population predicted to approach nine billion within the next fifty years, environmentalists and others are concerned about the planet's ability to absorb the additional load of greenhouse gasses entering the atmosphere and wreaking havoc on ecosystems on the ground. A combustion process using in industrial and power plant sectors is one of the main causes, as it has emitted 65% CO_2 of entire energy consumption sectors in Thailand, in year 2022. There are numerous ways to reduce CO_2 emissions from burning different types of fuel, including coal and fuel oil. Biomass fuel is a well-known substitute for these fuels, as it is cheaper, more accessible, and a renewable energy source that can be used to replace other fuels.

Albeit biomass fuel CO_2 emissions are relatively lower when it is used as the fuel for industrial boilers that produce steam for the system, compared to other types of fuel, they frequently encounter numerous difficulties. Fly ash that clings to the surface of the superheater tubes and causes fouling, corrosion, and erosion is a significant issue caused by biomass fuel. Due to these factors, additional funds will be required to cover this portion of the damage. Ultimately, a pilot scale design for measuring ash deposition on superheater tubes will be created.

Figure 1.1 Superheater tubes in a coal fired boiler.
(https://www.klayenersol.com)

1.2 Objectives

1.2.1 To study and design the pilot scale of superheater tubes in a water-tube boiler for ash deposition measurement (fouling and slagging problems). Implement engineering knowledge including thermodynamics, heat transfer, and fluid mechanics.

1.2.2 To study physical and chemical phenomena that cause ash deposition.

1.2.3 To create a test kit at a pilot scale for 3D design, including all the required equipment.

1.3 Hypotheses

1.3.1 The use of fuels containing inorganic components especially biomass (alkaline, alkaline earth), such as straw, wood, and bagasse, causes the ash deposition problem at superheater tube.

1.3.2 Capable of implementing the accumulated knowledge to the pilot-scale design using Heat Transfer fundamental.

1.4 Project Scopes

1.4.1 Ash deposition is caused by biomass fuel.

1.4.2 This project focused on ash deposition at the superheater tubes, a high-temperature region in industrial water-tube boilers, with a specific focus on fly ash.

1.4.3 In this study, the superheater tubes parameters (e.g., diameter, area) were calculated using actual data from a YOSHIMINE industrial water-tube boiler having capacity of 80 ton/hr.

1.4.4 The Boiler was running at 89.5% of its capacity at the thermal efficiency of 52.43% based on high heating value and 68.1% based on low heating value, where the combustion was taken place with 100% bagasse.

1.4.5 The heat transfer mode of the superheater tubes are conduction and convection with cross flow pattern.

1.5 Procedures

1.5.1 Define the topic, objective, and scope of the project.

1.5.2 Study about fuel and combustion mechanism of biomass.

1.5.3 Study the mechanisms of ash deposition and the chemical reaction of inorganic constituents released during combustion based on prior research.

1.5.4 Review engineering knowledge including heat transfer and thermodynamics to design the conceptual superheater tubes.

1.6 Expected Outcomes

1.6.1 The conceptual calculation of heat transfer in superheater tube.

1.6.2 A drawing construction for a pilot-scale design of ash deposition measurement.

CHAPTER 2
LITERATURE REVIEW

Due to Thailand's rapidly expanding economy, energy consumption has increased at a rapid rate in recent years. Oil, coal, and natural gas, among other fossil fuels, are utilized as sources of energy. These energy supplies are insufficient to match the demand, so they must be imported. Currently, renewable energy sources such as biomass, wind, sun, and hydropower are not widely utilized. Biomass can be considered by the industry as an alternative fuel to reduce environmental effects and save money. However, attention must be paid to the effects of using biomass as an alternative fuel. Prior scientific studies provide information regarding the impact of biomass fuel, as well as its issues, mechanisms, and analyses. The biomass fuel induces some major problems, the ash deposition occurs, and it will reduce heat transfer efficiency in the furnace walls and cause the steel surface to corrode over time, which is the primary cause of high maintenance costs and short lifespans.

Table 2.1 The selected study dealing with ash deposition mechanism, composition [1]

References	Fuel	System detail	Method	Finding
T. Madhiyanon et al 2012	-Empty fruit bunch (EFB)	Laboratory scale reciprocating grated fire 150 kw combustor	Utilized the biomass fuel in furnace with varying combustion temperature	Ash deposition mechanism
			Collect ash sample to analyses with XRF and SEM/EDX method	The chemical composition of ash in different location

References	Fuel	System detail	Method	Finding
				such as fly ash, bottom ash, deposit ash
			Measure by installed probe Attach load cell to the probe where the ash is deposited	-The thermal resistance of fouling -Heat uptake of steel surface Change in deposit mass
Tae-Yong Jeong et al 2019	-Bituminous coal -Empty fruit bunch (EFB) -Wood pellets (WP)	Co-combustion of pulverized coal with EFB, WP	Drop tube furnace (DTF) and deposition probe	The ash deposition tendencies of with different blend ratio of biomass fuel
			XRF	The chemical composition of laboratory

References	Fuel	System detail	Method	Finding
				and combustion ash
Lei Ma et al 2022	-Bark, peanut shell, and crushing material	35 Mw biomass fired powerplant	Developed a measurement apparatus with transformable cooling media, using SEM to analyze the ash	Four typical ash deposition layers

T.Madhiyanon et al. [1] have conducted a laboratory-scale experimental kit to investigate ash deposition with a 150 kw reciprocating grate fire combustor, variable speed drive, and a 35 mm carbon steel superheater. By utilizing EFB fuel, which has the highest K and Cl dry basis compared to other types of biomasses, serious slagging and fouling are expected.

They discovered that superheater surface deposition begins with the condensation of inorganic vapor containing KCl, followed by the inertial impaction of fly ash Si Ca. The deposition on both the inside and outside is composed primarily of KCl, with Si and Ca serving as secondary components. The appearance of the deposit is as shown in the picture:

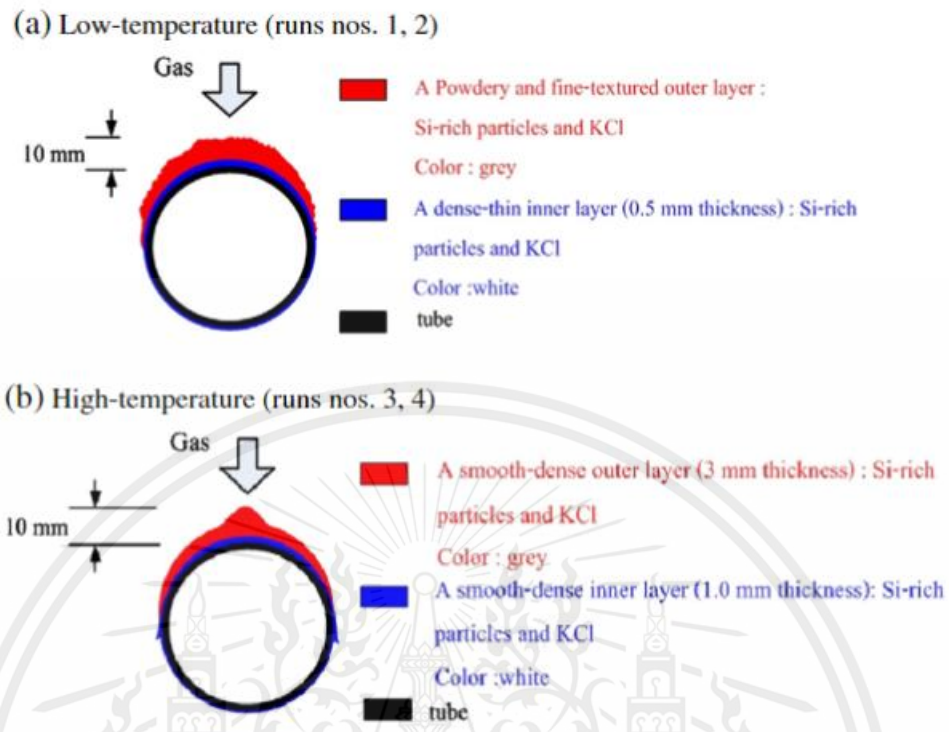

Figure 2.1 The appearance of the deposit

Experiments	Upstream Temperature (°C)	Deposit Probe		
		Upstream side	Lateral side	Downstream side
Low-temperature (run no.1)	606			
Low-temperature (run no.2)	612		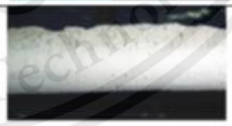	
High-temperature (run no.3)	843			
High-temperature (run no.4)	868			

Figure 2.2 The ash deposition at different operate temperature

T. Madhiyanon et al. [1] conducted an experiment on EFB combustion using the conditions listed in Table 2.2. They discovered that fouling deposits accumulate over time and that the total thermal resistance increases.

Table 2.2 The experiment condition T. Madhiyanon et al. [1]

Run	Condition	Combustion Temperature (°C)	Flue gas enter (°C)	Tube surface Temperature (°C)	Time (hr)	Deposit Flux (g/m^2h)
1	Low temp	794	606	300-425	28	182
2	Low temp	802	612	340-430	20	175
3	High temp	905	843	450-505	20	160
4	High temp	954	846	400-500	19	167

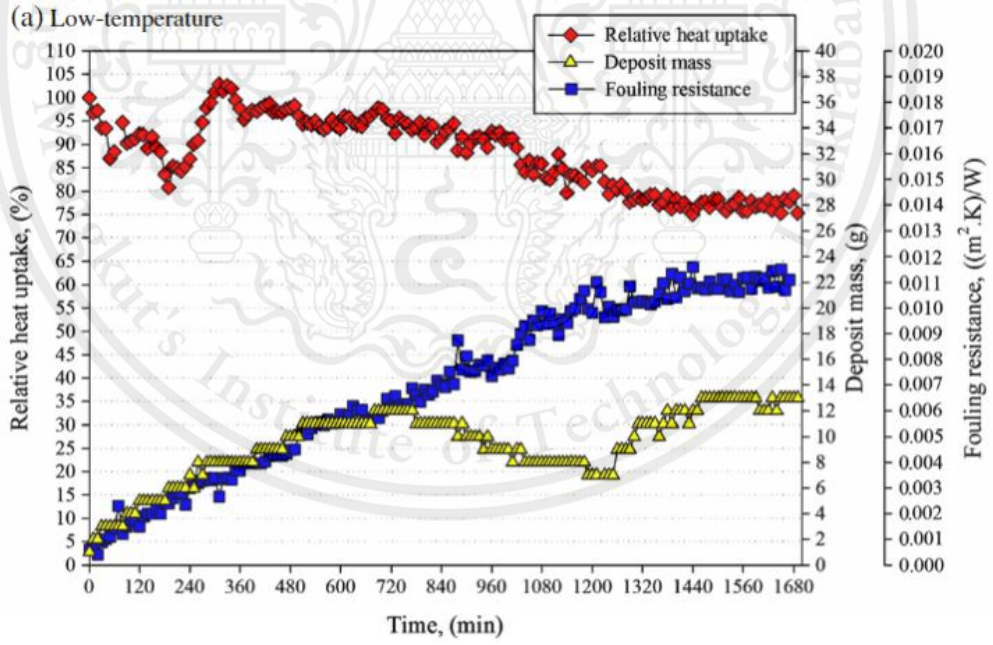

Figure 2.3 The relative heat uptake, deposit mass, fouling resistance in the function of time of low-temp experiment.

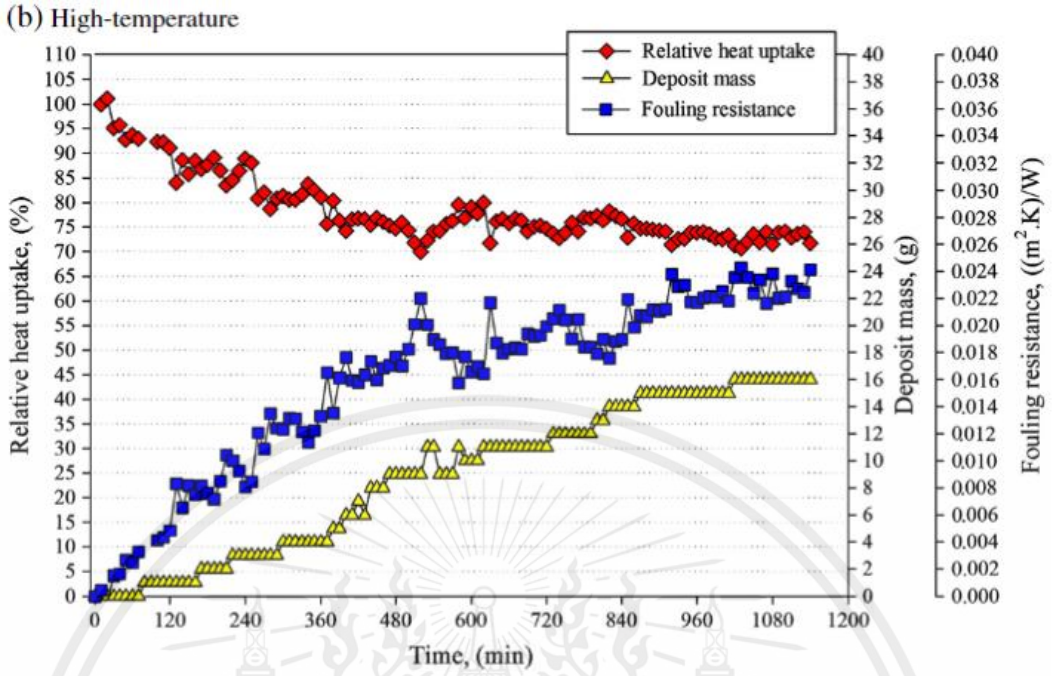

Figure 2.4 The relative heat uptake, deposit mass, fouling resistance in the function of time of high-temp experiment

The result shown in Figure 2.4 follows the same trend as combustion at low temperatures; however, the thermal resistance of deposits is higher. Thus, the increase in thermal resistance of the deposit is due to the KCl which has melted to strengthen and thicken it.

Low-temperature experiment (790-800°C) and High-temperature experiment (900-950°C) are the two parts of the experiment that are categorized by temperature. Then, the ash from the combustion process, such as fly ash and bottom ash, will be analyzed using XRF and SEM/EDX technologies with a deposit probe to determine the chemical constituents.

According to figures 2.5 and 2.6, the chemical composition of ash's elements differs when the same type of fuel is burned at different temperatures by varying the mass flow rate to control the combustion temperature. Because of temperature on the vaporization rate of the inorganic components of the fuel, a higher temperature will result in a more efficient vaporization of potassium than a lower temperature. Potassium content in

bottom ash is reduced by 40-60 wt.%, according to the analysis result. The high temperature produces intense chloride potassium vaporization.

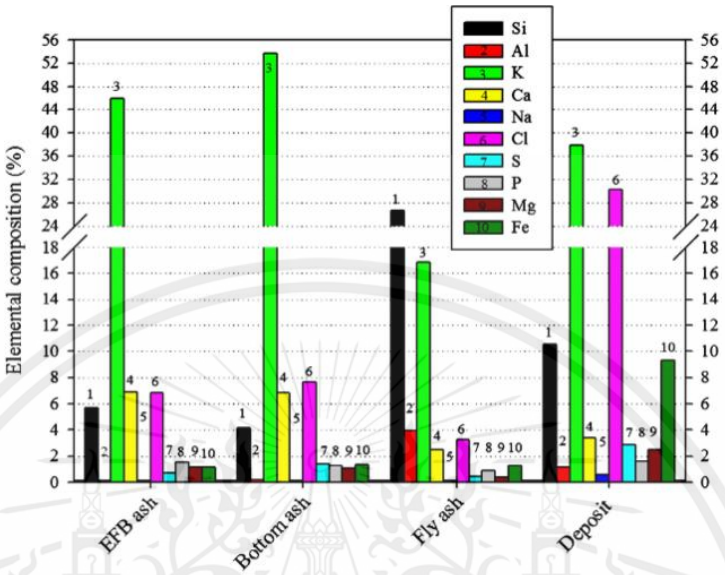

Figure 2.5 The composition of different position of ash of low temperature combustion

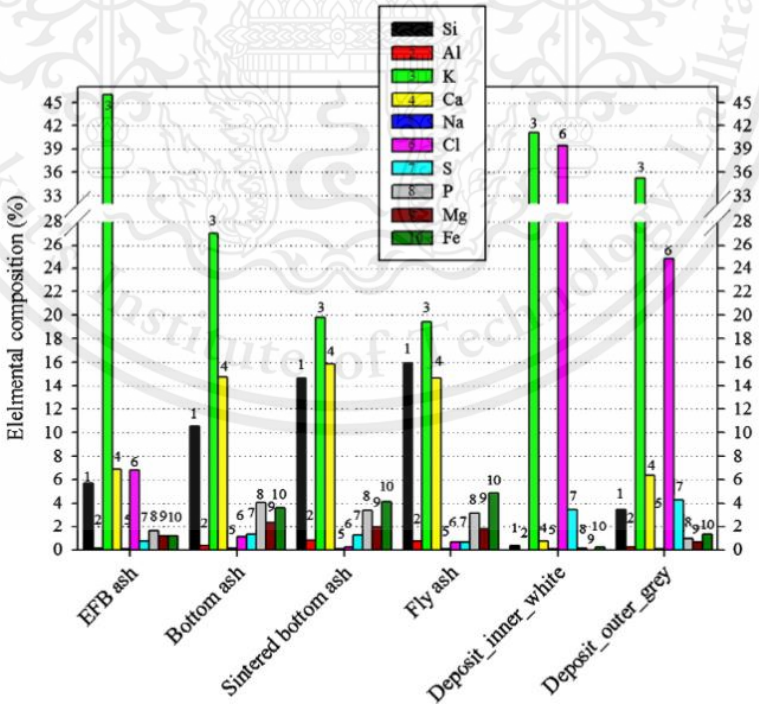

Figure 2.6 The composition of different position of ash of high temperature combustion

Tae-Yong Jeong et al. [11] performed an experiment to investigate the ash composition in biomass co-combustion. he concludes that the basic oxide in ash which can be detect by XRF is causing by increase in blend ratio of biomass fuel WP, EFB.

The DTF results show that a lower tendency of ash deposition can be obtained by using a blend fuel containing 10% WP and 15% EFB. As a result of the increased proportion of WP and EFB, the tendency for ash deposition will begin to increase.

Lei Ma et al. [12] designed a test system with transformable cooling media for ash deposition test and installed it between a precipitator and an air preheater. They analyzed the ash sample by using scanning electron microscope (SEM) with X-ray spectroscopy (EDS) and X-ray diffraction (XRD).

They identify ash deposition based on the appearance characteristics and degree of adhesion to the heating surface to examine the formation mechanisms as four groups: dry-loose ash layer, multi-loose ash layer, adherent ash layer, and viscous ash layer.

Observations under varying heating surface temperatures (T_w) between 40°C and 140°C (as shown in Figure 2.7) reveal that a drop in temperature results in sticky ash deposition on the windward side and wet ash on the leeward side. When removing ash layers, ash begins to adhere more strongly, becoming more difficult to remove, and develop corrosion spots. At temperatures below 50°C, ash deposition forms a fish-scale pattern; the outside layer is easily removed, while the inner layer adheres to the pipe surface and causes corrosion.

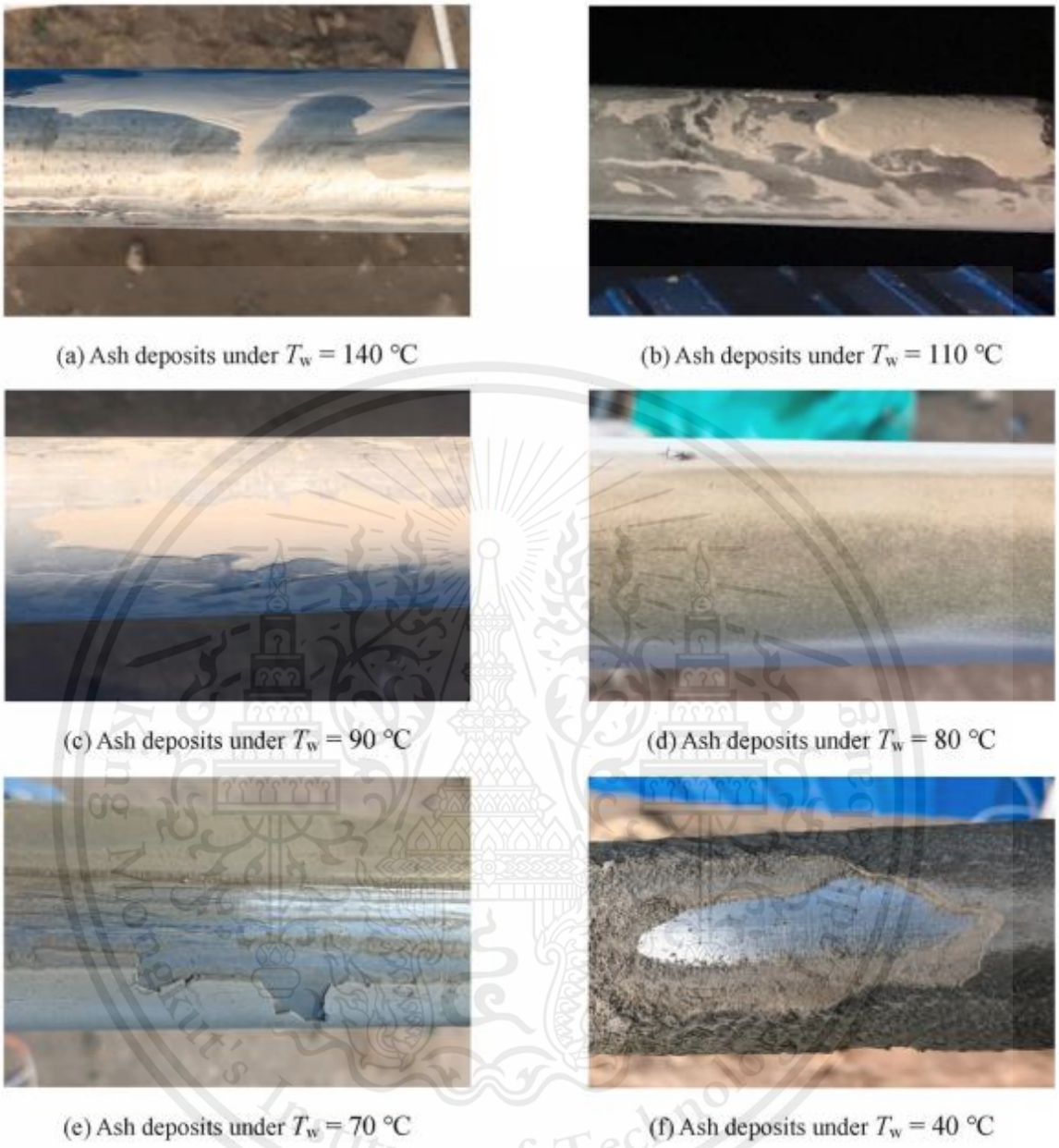

Figure 2.7 Samples of ash deposition on pipe [12]

CHAPTER 3

THEORY

3.1 Boiler

A boiler is a vessel capable of producing steam in the desired quantity or pressure for various industrial applications. Therefore, boilers are designed to accommodate a variety of applications, including saturated steam for heat exchangers in manufacturing and superheated steam at high temperature and pressure for power plants. [3]

3.1.1 Boiler type

3.1.1.1 Water Tube Boiler

Contain tubes filled with water that allow water to flow through a firebox that is heated. The upper drum, the steam drum, and the lower drum, the mud drum, are connected by tubes in water tube boilers. The boiler feedwater that enters these drums has chemicals added to it to stop corrosion and fouling. A direct-fired heater with a natural gas, oil, or combination burner produces heat in the boiler. The water tubes get the heat from the burner. The combustion gas heats the water as it passes through the tubes and creates steam. While combustion gas is released from the boiler stack as flue gas, this steam is collected in the upper drum.

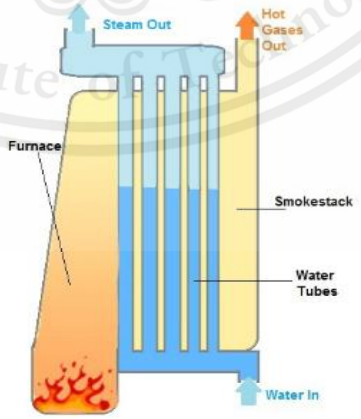

Figure 3.1 Water tube boiler diagram

(https://www.globalspec.com)

Figure 3.2 Water tube boiler

(https://getabecboiler.com)

3.1.1.2 Fire Tube Boiler

The furnace is where the fuel is burnt to produce hot gases and they will be sent to pass through the fire tube. The fire tubes are submerged in water inside the main tank and begin with the transfer of heat energy of hot gases to the surrounding water as they travel through the tubes. Steam is generated in the water, which will rise to the surface, and it will be kept inside of the vessel of the same fire tube boiler.

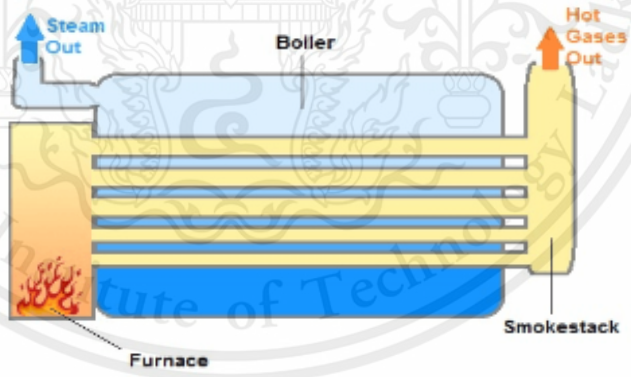

Figure 3.3 Fire tube boiler

(https://www.globalspec.com)

Figure 3.4 Fire tube boiler

(https://getabecboiler.com.vn)

3.1.1.3 Hybrid Boiler

A hybrid boiler is a vessel that has both water tubes and fire tubes. The combustion chamber for solid fuel will have a water-tube boiler section at its base. The fire tube boiler, which will receive the excess heat from the water tube boiler's ventilation pipe, will be located at the top.

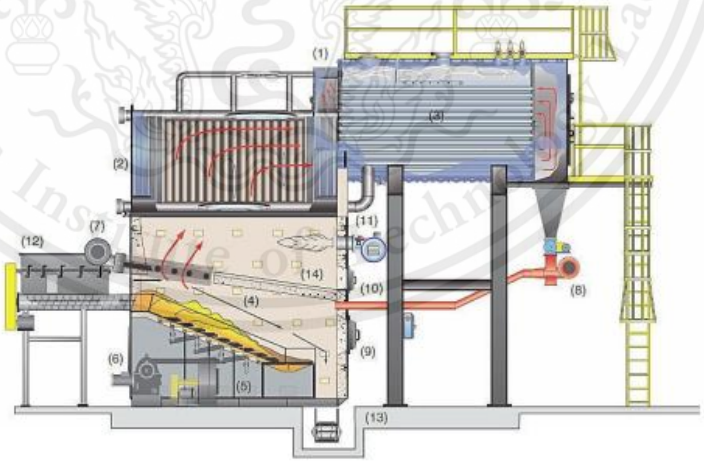

Figure 3.5 Hybrid boiler

(http://reg3.diw.go.th)

3.1.2 Thermodynamics in boiler

The first law of thermodynamics is about fundamental energy conservation. The boiler will consider at open system, steady-state steady-flow (SSSF).

Energy conservation equation [6]:

$$\dot{E}_{in} - \dot{E}_{out} = d\dot{E}_{sys} \tag{3-1}$$

The total energy of an open system (control volume) is constant during a steady-flow process. Therefore, equal amounts of energy must enter and exit a control volume. For a steady-flow process, the rate form of the general energy balance can be written as:

$$E_{in} = E_{out} \tag{3-2}$$

The rate form of conservation of energy expressed as:

$$\dot{E}_{in} = \dot{E}_{out} \tag{3-3}$$

Where the total energy that transport by mass of SSSF system composed with 3 forms that is enthalpy, kinetic energy, and potential energy.

$$E = H + \frac{1}{2}mv^2 + mgz \tag{3-4}$$

In terms of mass basis:

$$e = \frac{E}{m} = h + \frac{1}{2}v^2 + gz \tag{3-5}$$

Equation of conservation of mass or continuity equation:

$$\dot{m}_{in} = \dot{m}_{out} \tag{3-6}$$

The mass flowrate of one-dimensional flow approximation can be expressed as:

$$\dot{m} = \rho v A_c \tag{3-7}$$

The volumetric flow rate can be expressed as:

$$\dot{V} = vA_c = \frac{\dot{m}}{\rho} \tag{3-8}$$

First law of thermodynamics suggest energy analysis for steady state steady flow can be written as:

$$\dot{E}_{in} = \dot{E}_{out} \tag{3-9}$$

$$\dot{Q}_{in} + \dot{W}_{in} + \dot{m}_{in}(h + \frac{1}{2}v^2 + gz)_{in} = \dot{Q}_{out} + \dot{W}_{out} + \dot{m}_{out}(h + \frac{1}{2}v^2 + gz)_{out} \tag{3-10}$$

Neglecting the change in kinetic energy and potential energy and there is no boundary work in boiler, The conservation of energy reduces to:

$$Q = m(h_2 - h_1) \tag{3-11}$$

Pure substance refers to the substance which composed with fix chemical element such as water and nitrogen. In boiler, the flowing liquid is water, thus the property of water will be described.

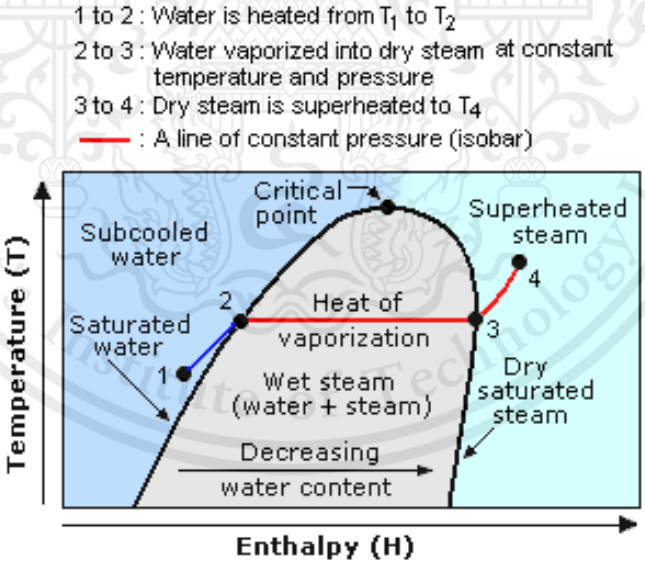

Figure 3.6 T-H Diagram of water to steam (converting water into superheated steam)
(https://www.enggcyclopedia.com/2019/04/superheated-steam)

3.1.3 Boiler efficiency

The heat efficiency of boiler can be calculated by direct method and indirect method.

For direct method:

$$\eta_{th} = \frac{output}{input} \cdot 100 = \frac{m_w(h_{steam} - h_{fw})}{m_f(HV)} \cdot 100 \quad (3\text{-}12)$$

Where HV is heating value of the particular fuel depend on the state of water in combustion products. HV can be categorized into 2 groups depending on the phase of water which is the product of combustion [6].

Heating value is referred to the lower heating value (LHV) when the water in the combustion product entirely evaporates that mean some of heat output were sharing to the water, or in case of water in combustion product is totally liquid phase, the heating value will be known as higher heating value (HHV) since all of heat output was presence.

The relation of HHV and LHV can be expressed as:

$$HHV = LHV + (mh_{fg})_{H_2O} \quad (3\text{-}13)$$

Where m represents mass of water in combustion product

h_{fg} is the different between enthalpy of gas phase and liquid phase of water at specified temperature

For indirect method {8]:

$$\eta_{th} = \frac{output}{input} \cdot 100 = (1 - Loss) \cdot 100 \quad (3\text{-}14)$$

Heat loss in boiler referenced from JISB8222 consists of the heat loss composed of the heat loss from dry exhaust gas (L_1), the heat loss from incomplete combustion (L_2), the heat loss in the unburnt fuel (L_3), heat loss from radiation (L_4), heat loss from the blowdown (L_5), and other heat loss (L_6). The equation can be written as:

$$Loss = L_1 + L_2 + L_3 + L_4 + L_5 + L_6 \quad (3\text{-}15)$$

3.2 Combustion of biomass

3.2.1 Solid fuel combustion

When the particles are heated by hot air, mass of the fuel will be decreasing over the three phases, which are [4]:

(i) **Drying** means chasing the moisture out at the appropriate temperature. The fuel particles are disintegrated by heat or pyrolysis. There are two sorts of water within the fuel: free water and bound water.

(ii) **Devolatilization** is when the products are combustible organic matter and char.

(iii) **Char combustion** happens after pyrolysis while the volatile substance and char are burnt at the same time.

The chemical equation of combustion of fuel such as C_xH_y with theoretical air can be expressed as [5]:

$$C_xH_y + a_{th}(O_2 + 3.76N_2) \rightarrow xCO_2 + (y/2)H_2O + 3.76a_{th} \quad (3\text{-}16)$$

Where $$a = x + y/4 \quad (3\text{-}17)$$

For fuel composed with $C_xH_yO_z$ the chemical equation can be expressed as:

$$C_xH_yO_z + a_{th}(O_2 + 3.76N_2) \rightarrow xCO_2 + (y/2)H_2O + 3.76a_{th} \quad (3\text{-}18)$$

Where $$a = x + \frac{y}{4} - \frac{z}{2} \quad (3\text{-}19)$$

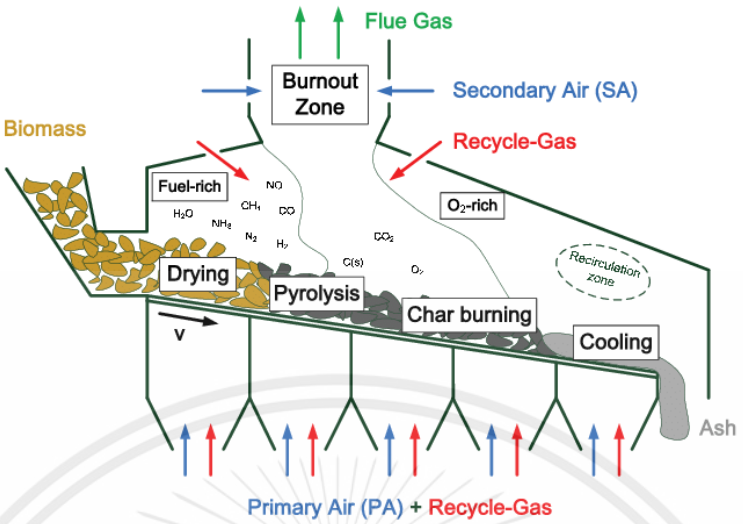

Figure 3.7 Solid Fuel Combustion

(https://www.researchgate.net)

3.2.2 Biomass fuel combustion

Biomass combustion is close to that of the low-quality carbon coal (has a lot of volatile substances), including heating, drying, and devolatilization or pyrolysis, then creating volatile substance and char.

1. Heating and drying

The moisture will vaporize at temperatures (< 100°C); however, the evaporation of moisture requires the heat emitted by combustion, which lowers the temperature of the combustion chamber and slows the combustion process. For example, the combustion stability inside the boiler cannot be maintained if the wood's moisture content surpasses 60% (wet basis).

The adiabatic flame temperature will drop in proportion to the moisture content, the increase in ash, and the increase in theoretical air.

2. Devolatilization or pyrolysis

Pyrolysis happens during the initial phase of biomass combustion and plays an important role in the combustion process. Since 80% of biomass is converted into volatile products, pyrolysis is considered a slow chemical reaction at low temperatures, occurring at 160-250 ^{o}C for biomass and 350 ^{o}C for bituminous coal.

Devolatilization rate of biomass expressed as overall reaction rate equation [4]:

$$-\frac{dm_v}{dt} = m_v A_v \exp -\frac{E_A}{R_u T} = m_v k \quad (3\text{-}20)$$

Where m_v refer to devolatilization mass t refer to time E_A refer to activation energy

A_v refer to a factor exponential of devolatilization,

k refer to reactivity $= A_v \exp \frac{-E_A}{R_u T}$

3. *Char combustion*

The remainder from the pyrolysis process is char, which performs a heterogenous reaction with the gaseous. Mass transfer of oxygen to the carbon surface can occur via O_2, CO_2 and H_2O.

Chemical reaction of combustion homogeneous may be performed by one or more of the reactions listed below.

$$C + \frac{1}{2}O_2 \rightarrow CO$$
$$C + O_2 \rightarrow CO_2$$
$$C + CO_2 \rightarrow 2CO$$
$$C + H_2O \rightarrow CO + H_2$$

3.3 Ash composition, formation, and deposition

3.3.1 Ash composition

Ash composition of biomass can be found by bringing the analyzing the ash sample for the chemical compositions. Typically, the ash sample from the ashing will be used at temperature 550 ^{o}C for biomass fuel and 750-800 ^{o}C for fossil fuel. Under the hypothesis that the inorganic matter is in the form of oxide inside the ash. Thus, the report about the analysis of ash compositions in oxide form is common. From the table with different kinds

of biomass, the ratio of inorganic matter is quite varied unlike organic matter. Overall, the ash of biomass is mainly composed of Si, Ca, and K. [4]

Table 3.1 The ash compositions of different kinds of biomass [5]

Elements in ash wt.% db.	Husk	Eucalyptus wood	Bark	Empty fruit bunch (EFB)	Palm fiber	Palm kernel shell
Si	92.5	16.72	7.20	9.34	26.57	15.15
Al	0.20	16.38	2.52	0.23	0.73	0.44
Ti	0.01	2.93	0.11	N/A	0.14	0.05
Fe	0.34	2.52	1.20	N/A	2.39	0.79
Ca	0.77	24.53	63.34	11.37	22.63	75.75
Mg	0.45	5.86	10.09	1.89	5.69	1.19
K	4.88	14.45	11.84	75.96	28.87	4.61
Na	0.05	15.61	2.12	0.11	0.35	0.18
S	0.30	1.01	N/A	1.10	3.54	0.51
P	0.52	N/A	1.58	N/A	9.09	1.33
Total	100	100	100	100	100	100

Table 3.2 The properties of biomass fuel [4]

Fuel type	Ash content wt.% db.	Major ash forming elements
Bituminous coal	3-25	Si, Al, Fe
Lignite	5-40	Si, Al, Ca, Mg, Fe, S
Herbaceous biomass	4-12	Si, K, Ca, and high Cl
Woody biomass	0.5-7	Ca, K, Si, Mg
Manure and sludges	15-50	Ca, P, Si, Na, S

Municipal solid waste (MSW)	5-45	Diverse composition, frequently abundant in Cl and heavy metal

3.3.2 Ash formation

In biomass combustion, a portion of the ash generating elements in the biomass fuel are vaporized. The proportion of volatile matter is dependent upon the characteristics of the biomass, the combustion environment, and the combustion technology.

Once the substances become gas, their particles will be very small within the boundary layer of coal particles, which are experiencing the burning of re-oxidation and nucleation processes, respectively.

Primary particle that comes from the vaporization of volatile substance and nucleation within the boundary layer will have the size around 5-10 nm. However, in the process of transporting along with the flu gas, the particles are bigger from coagulation, agglomeration, and condensation process. These particles are in the basic mode of small particles formation in fly ash called aerosol (particle size <1 μm).

The compounds, which are not vaporized and left inside the carbon coal, start to melt, and combine. The result yields the ash after combustion which contains various components, size, and shape inside of the fuel.

The proportion of ash which are blown along with the exhaust gas and rough particles (>5 μm) depends on the density, particle size, combustion technology, and velocity while the rest become the bottom ash inside the combustion chamber.

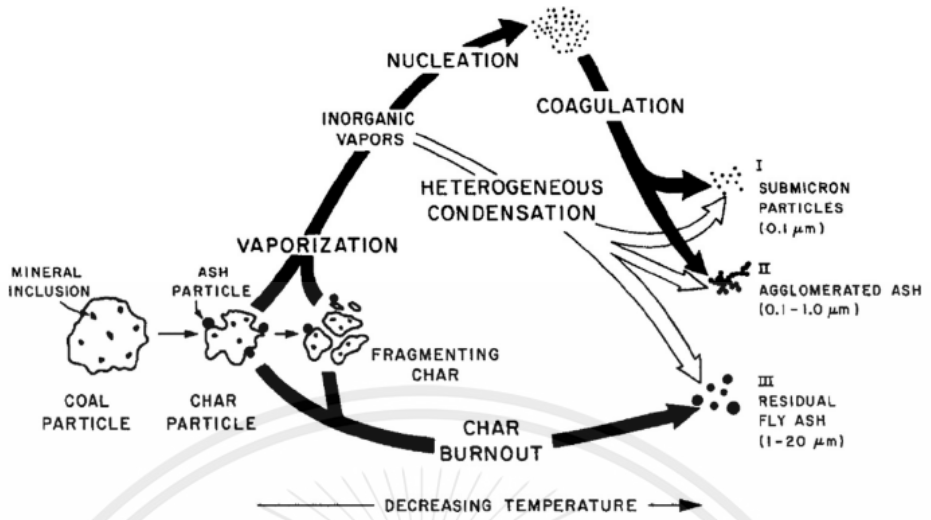

Figure 3.8 Ash formation from solid fuel combustion [4]

3.3.3 Ash deposition mechanisms

Inorganic constituents in biomass are separated into 3 groups [5]:

1. Inorganic matter is commonly distributed inside the organic structure of the fuel.
2. Inorganic matter, small mineral particles, are embedded inside the fuel particle.
3. Inorganic matter that are impure substances.

Inorganic matter in fuel which turned into fly ash can be categorized to 2 groups:

1. A group that formed from inorganic release mechanisms.
2. A group in the form of ash.

The mechanism for the release of inorganic matter involves 1) volatilization 2) inorganic substance reaction resulting from devolatilization by heat and chemical reactions 3) organic substance reaction with organic matter that evaporates from fuel. As for biomass, K and Na are examples of inorganic volatile substances.

The mechanism generates small particles ($< 0.1\ \mu m$), whereas the residual vapor of an inorganic substance transforms into larger ash particles via physical and chemical processes, depending on chemical components, combustion temperature, and combustion time.

Ash deposition depends heavily on the presence of ash particles or inorganic vapors on heat exchanging surfaces. Particle deposition includes particle transport to the wall, particle impact, and particle impaction, often known as particle sticking.

The transport mechanisms which cause ash deposition on the surface includes, Inertial impaction, Thermophoresis, Condensation, and Chemical reaction, can be explained as:

Inertial impaction [4]

Fly ash with diameter more than 10 μm have higher inertia, when inertia force is more than aerodynamic force the particle cannot follow the streamline. The particles will make an impact with the pipe surface, some of them can be embedded to the surface. Most of the impact happens at stagnation point, I. This behavior can be expressed by Stoke number:

$$St^c = \frac{\rho_p d_p^2 u_p}{9\mu_g d_c}\psi \quad . \qquad (3\text{-}22)$$

ψ correction factor is the function of particle Reynolds number $\mathbf{Re}_p$ which can be expressed as

$$\psi(\mathrm{Re}_p) = \frac{3\cdot(\mathrm{Re}_p^{1/3}\cdot\sqrt{0.158} - \tan^{-1}(\mathrm{Re}_p^{1/3}\cdot\sqrt{0.158}))}{\mathrm{Re}_p\cdot 0.158^{3/2}} \qquad (3\text{-}23)$$

And particle Reynolds number $\mathbf{Re}_p$ expressed as

$$\mathrm{Re}_p = \frac{\rho_g \cdot d_p \cdot u_p}{\mu_g} \qquad (3\text{-}24)$$

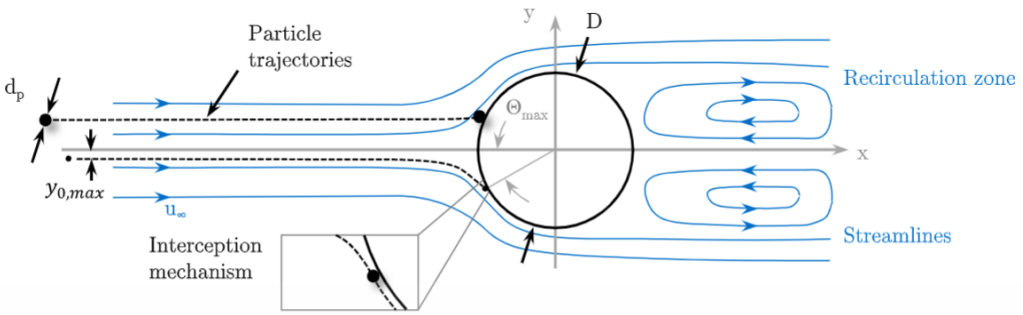

Figure 3.9 Inertial impaction [4]

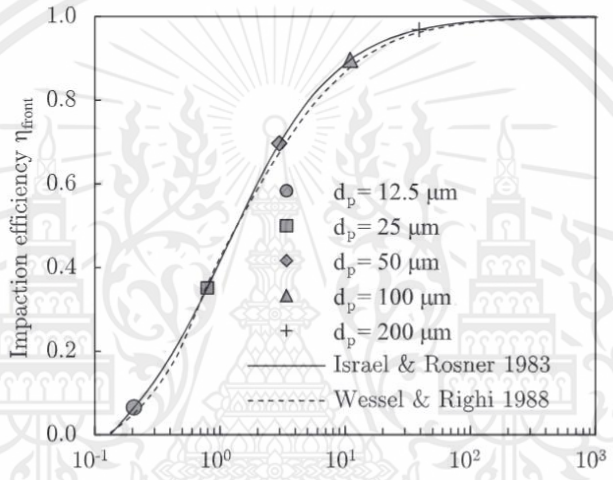

Figure 3.10 Impaction efficiency which equals to mass of impacting particle over the total flowing mass [4]

Thermophoresis [4]

Thermophoresis (TP) is explained by the varying bombardment of gas molecules on a particle's surface. On the hot side of a particle, the kinetic energy of gas molecules is greater than on the cool side. The greater kinetic energy of collisions between molecules and the surface of a hot particle results in a net force acting on the particle in the direction of the cold flow.

Action force from thermophoresis can be calculated by:

$$F_T = -6\pi\mu_g d_p f(Kn)\nabla T_g \tag{3-25}$$

Where $f(Kn)$ depend on particle diameter, Knudsen number and specific properties available in the research of Baxter and Hardesty (1992a) and (1992b).

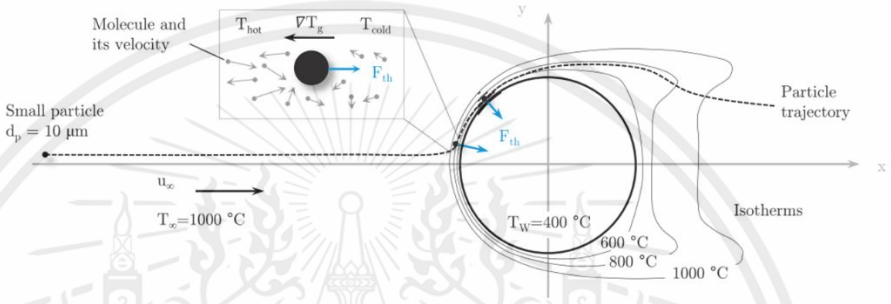

Figure 3.11 Thermophoretic force acting on particles in thermal boundary layer of heat exchanger surface [4]

Condensation [4]

Condensation is the mechanism by which inorganic vapor condenses at a surface temperature lower than the gas temperature. The quantity of condensed condensate depends heavily on the mode of inorganic formation in fuel. Coal and low-grade biomass have a greater tendency to form condensate, but high-grade coal has a lesser tendency.

When inorganic vapor condenses at the surface, it transforms into a viscous fluid that traps the tough, difficult-to-remove deposit particles.

Inorganic vapor entering the boundary layer with a cooler surface will condense via 3 mechanisms:

1. Inorganic vapor cross flow and homogenous condensed on surface or deposit.

2. Inorganic vapor condensed, homogeneous nucleation into fume, and induced by thermophoresis.

3. Inorganic vapor heterogenous condensed on other particle induced by thermophoresis.

Na In comparison to thermophoresis and inertial impaction, condensation deposit particles <0.5 μm that attach evenly to the surface. The deposit particles of condensation are sticky and increase the chance of capturing particulate matter. These particles typically consist of K Cl and occasionally Na.

Chemical reaction [4], [10]

The chemical reactions are sensitive to temperature. It can be determined by chemical reactions whether a particle attaches, and a deposit begins to develop. This is the result of the heterogeneous interactions involving deposits and gas species. The closest chemical reactions to ash depositions include: (i) oxidation, (ii) Sulfation, compounds that contain alkali metals (K or Na) are the primary sulfating species. Both reactions can either occur as a gas phase reaction, or as gas-solid reaction. In addition, they emit chlorine species that can attack the metal surface and cause corrosion, (iii) Alkali absorption, leads to a formation of low-melting silicates. The transformations can include sintering and strongly affect physical properties of the deposit, depending on the temperature, and (iv) Eutectics, formation of low temperature eutectics (a mixture or substance that melts and solidifies) from the interaction of Fe, Na, Ca, Al, and Si.

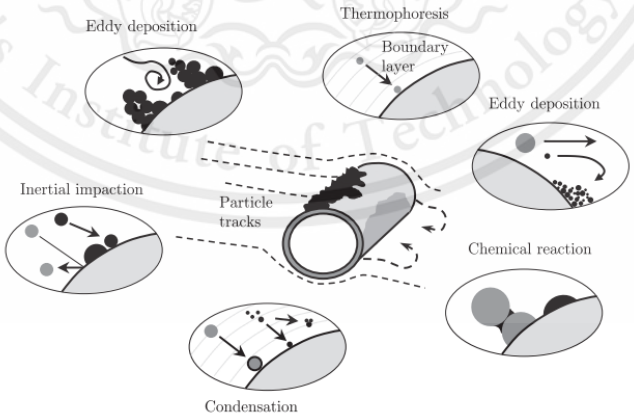

Figure 3.12 Ash was deposited by the transport mechanism on the heat exchanger surface. [2]

Deposition rate for inorganic matter species i at specific time t can be expressed as:

$$\frac{dm_i}{dt} = I_i(\tau,t)G_i(\tau,t) + T_i(\tau,t) + C_i(\tau,t) + R_i(\tau,t) \quad (3\text{-}26)$$

Where the inertial impaction rate, G_i is capture efficiency of particle, T_i Deposition rate cause by thermophoresis and R_i is chemical reaction rate and I_i impaction rate of inertia force. [5]

3.4 Slagging, fouling, and their effects

Slagging deposition happens at the furnace wall and the surface of the combustion chamber, including the burner. Slagging is composed of inner layer in powdery deposits and molten ash in many layers. The deposits on the surface of the furnace are silicate, iron, and the alkali group. Slagging decreases the heat absorption ability of the furnace, raises the temperature of the exhaust gas, and causes the overheating of superheater tubes, which will lead to the ash deposition around the heat transfer area.

Fouling occurs around the heat transfer area on superheater tubes. This phenomenon is about the condensation of the volatile substance in the fire, occurs between different temperature ranges depending on the different inorganic matter in the exhaust gas. Thus, the inner layer of the ash on the tubes are mostly alkali salts, which can catch the other particles.

Corrosion of superheater [4]

Alkali chlorides deposited on superheater tubes are well-known to cause corrosion in boilers that burn biofuels and waste, and they are also the primary factor that limits the final steam temperature and, thus, the efficiency of biofuel and waste boilers. Corrosion occurs in the following situations [9]:

In oxidation atmosphere, metal gradually oxidizes and forms a smooth and dense oxide scale adjacent to the metal. The oxide scale provides a barrier for further diffusion

of oxygen and most other gaseous species to the metal and, as a result, oxidation corrosion is limited.

In reducing atmosphere where oxygen is absent or insufficient, metal chlorides form directly on the metal surface. Therefore, the volatilization of metal chloride, which is strongly dependent on temperature, governs the rate of corrosion.

Erosion [4]

Erosion is the process that occurs when sharp, solid particles clash with non-adherent portions on the surface of a deposit. Typically, these are quartz particles with relatively high melting points found in coal-fired boilers. As a slow process of material removal, erosion can be split into deformation and cutting actions. Erosion of hard angular quartz particles, which cause erosion by cutting, and glass particles leading to surface deformation and brittle failure. Main parameters influencing erosion are particle hardness, shape, diameter, impact velocity, and angle of impaction. Erosion is the major process for removing dry, powdery deposits, molten slags are not altered by erosion.

3.5 Heat transfer [7]

Heat transfer is thermal energy that is transported by the driving force of temperature difference. The direction of heat transfer is from higher temperature medium to lower. There are 3 modes of heat transfer 1) conduction 2) convection, and 3) radiation. Since a superheater is located next to the furnace zone, the heat transfer mode will be only conduction and convection.

3.5.1 Conduction

Conduction is the transfer of heat from one area of a material to another or to a material that it is in touch with. Heat is conceptualized as molecular activity, or, approximately, as the vibration of a material's molecules. When a portion of a material is heated, the vibration of its molecules increases. This stimulates higher activity in nearby molecules and initiates heat transport from the hotter to the colder portions of the substance. In addition to conductance through the metal of a tube, shell, or furnace, there

is significant surface conductance between a fluid and a solid in boilers, such as between water and a tube and gas and a tube. [1]

Rate of heat conduction can be expressed by Fourier's law:

$$\dot{Q}_{cond} = kA\frac{\Delta T}{L} \tag{3-27}$$

3.5.2 Convection

It is the process by which energy is transferred from a stationary solid surface to a moving liquid or gas nearby. It involves both the effects of conduction and fluid motion. Convection heat transmission increases with fluid motion speed.

Newton's cooling law state the rate of convection heat transfer as:

$$\dot{Q}_{convection} = hA_s(T_s - T_\infty) \tag{3-28}$$

Force convection

When a fluid is forced to flow over a surface by an outside force, such as a fan, pump, or the wind, the process is referred to as forced convection.

Considering the water in superheater tube, the flow of water can be classified as internal force convection. Firstly, the type of flow is required to determine whether laminar or turbulent flow.

The Reynolds number suggest:

$$\mathbf{Re} = \frac{\rho VD}{\mu} = \frac{4\dot{m}}{\mu\pi D} \tag{3-29}$$

The flow in tube is consider laminar for $\mathbf{Re}$ <2300, Fully turbulent for $\mathbf{Re}$ >10,000.

3.5.3 Overall heat transfer coefficient (U)

The modes of heat transfer in heat exchanger are conduction and convection. Convection occurs in the superheater tube of a water-tube boiler between flue gas and the steel surface and the steel surface with water inside the tube. Conduction heat transfer occurs from outer steel surface to inner steel surface.

Considering the thermal resistance network associated with superheater tube, there are 3 thermal resistances 1) inner thermal resistance R_i 2) wall thermal resistance R_{wall} 3) outer thermal resistance R_o, while the total resistance can be calculated by numerically summation of each thermal resistance which becomes.

$$R_{total} = R_i + R_{wall} + R_o = \frac{1}{h_i A_i} + \frac{\ln(D_o / D_i)}{2\pi kL} + \frac{1}{h_o A_o} \tag{3-30}$$

Combine all the thermal resistance into to single thermal resistance R_{total}

$$R_{total} = \frac{\Delta T}{\dot{Q}} \tag{3-31}$$

$$\dot{Q} = \frac{\Delta T}{R_{total}} = UA_s\Delta T = U_i A_i \Delta T = U_o A_o \Delta T \tag{3-32}$$

Canceling ΔT ,The R_{total} can be expressed as:

$$R_{total} = \frac{1}{UA_s} = \frac{1}{U_i A_i} = \frac{1}{U_o A_o} = \frac{1}{h_i A_i} + R_{wall} + \frac{1}{h_o A_o} \tag{3-33}$$

Consider the small thickness of heat exchanger tube ($A_i \approx A_o \approx A_s$) and high thermal conductivity material were used, the thermal resistance of wall R_{wall} can be estimated as ($R_{wall} \approx 0$), thus the equation for overall heat transfer coefficient U can be expressed as:

$$\frac{1}{U} \approx \frac{1}{h_i} + \frac{1}{h_o} \tag{3-34}$$

Where h_i is the inside convection heat transfer coefficient

h_o is the outside convection heat transfer coefficient.

For the used heat exchanger, the fouling is started to accumulate over the time as solid deposit build up on heat exchanger surface both inner surface and outer surface the R_{total} can be modified as

$$R_{total} = \frac{1}{UA_s} = \frac{1}{U_i A_i} = \frac{1}{U_o A_o} = \frac{1}{h_i A_i} + \frac{R_{f,i}}{A_i} + \frac{\ln(D_o / D_i)}{2\pi kL} + \frac{R_{f,o}}{A_o} + \frac{1}{h_o A_o} \quad (3\text{-}35)$$

Where $R_{f,i}$ is fouling factor at inner surface

$R_{f,o}$ is fouling factor at outer surface transfer coefficient.

Some of fouling factors for unit area surface were recorded at Table 3.3.

Table 3.3 The fouling factor of different fluid [7]

Fluid	Fouling factor R_f $(m^2 \cdot \frac{K}{W})$
River water, sea water, distilled water, boiler feed water	
Below 50 ^{o}C	0.0001
Above 50 ^{o}C	0.0002
Fuel oil	0.0009
Transformer, lubricating or hydraulic oil Steam (with oil traces) Organic solvent vapors, natural gas Refrigerant (liquid)	0.002

The heat transfer rate in heat exchanger that has both conduction and convection can be calculated as:

$$\dot{Q} = UA_s \Delta T_{lm} \quad (3\text{-}36)$$

Log mean temperature difference can be calculated as:

$$\Delta T_{lm} = \frac{\Delta T_1 - \Delta T_2}{\ln(\Delta T_1 - \Delta T_2)} \tag{3-37}$$

3.6 Pressure Loss and Head Loss [13]

In pipe flow analysis, the pressure drop ΔP is an important factor as it directly correlates with the energy needed from a fan or pump to sustain the flow.

The pressure loss in the superheater can be calculated as:

Energy equation:

$$\frac{P_1}{\gamma} + \frac{V_1^2}{2g} + z_1 = \frac{P_2}{\gamma} + \frac{V_2^2}{2g} + z_2 + h_{L,total} \tag{3-38}$$

Pressure loss:

$$\frac{P_1 - P_2}{\gamma} = h_{L,total}$$

$$\frac{\Delta P}{\gamma} = h_{L,total} \quad ; \quad V_1 = V_2, z_1 = z_2 \tag{3-39}$$

$$\Delta P = \gamma h_{L,total} \quad ; \quad \Delta P = P_2 - P_1$$

Head loss:

$$h_L = h_{L,major} + h_{L,minor} \tag{3-40}$$

Head loss major:

$$h_{L,major} = f \frac{1}{D} \frac{V^2}{2g} \tag{3-41}$$

Head loss minor:

$$h_{L,minor} = K_L \frac{V^2}{2g} \tag{3-42}$$

Reynold's number:

$$Re = \frac{\rho VD}{\mu} = \frac{VD}{\nu} \tag{3-43}$$

The friction factor can be calculated from:

$$\frac{1}{\sqrt{f}} = -2.0\log\left(\frac{\varepsilon/D}{3.7} + \frac{2.51}{Re\sqrt{f}}\right) \tag{3-44}$$

We can get the value of roughness (ε) from:

TABLE 8–2

Equivalent roughness values for new commercial pipes*

Material	Roughness, ε ft	Roughness, ε mm
Glass, plastic	0 (smooth)	
Concrete	0.003–0.03	0.9–9
Wood stave	0.0016	0.5
Rubber, smoothed	0.000033	0.01
Copper or brass tubing	0.000005	0.0015
Cast iron	0.00085	0.26
Galvanized iron	0.0005	0.15
Wrought iron	0.00015	0.046
Stainless steel	0.000007	0.002
Commercial steel	0.00015	0.045

* The uncertainty in these values can be as much as ±60 percent.

Figure 3.13 The equivalent roughness values for new commercial pipes.

We can get the value of K_L from Fig.12 and Fig.13

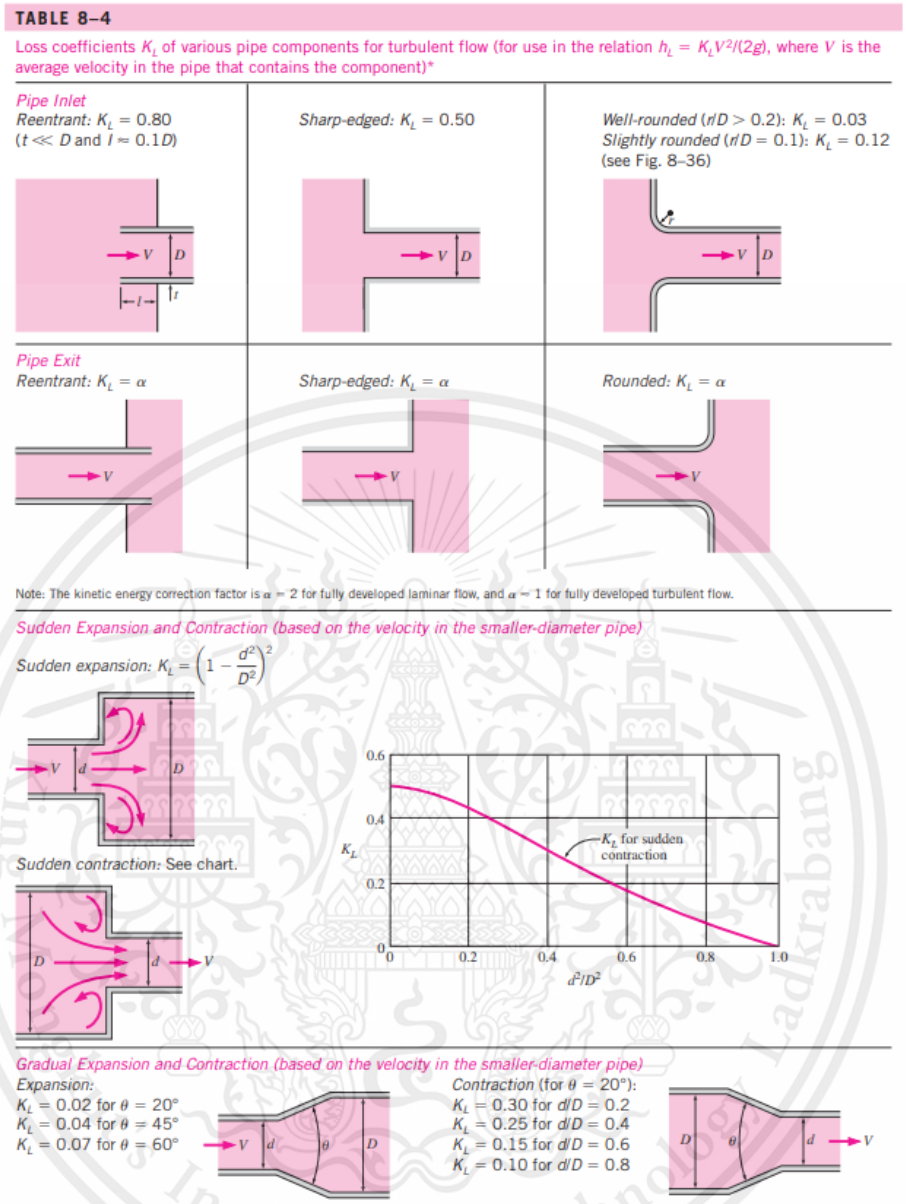

Figure 3.14 Loss coefficient K_L of various pipe components for turbulent flow.

TABLE 8–4 (CONCLUDED)

Bends and Branches

90° smooth bend:
Flanged: $K_L = 0.3$
Threaded: $K_L = 0.9$

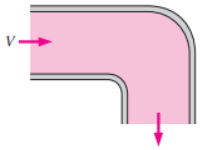

90° miter bend
(without vanes): $K_L = 1.1$

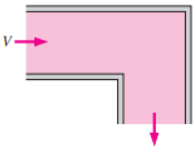

90° miter bend
(with vanes): $K_L = 0.2$

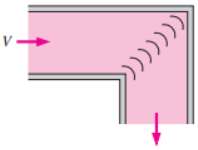

45° threaded elbow:
$K_L = 0.4$

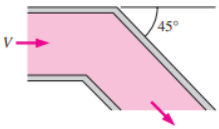

180° return bend:
Flanged: $K_L = 0.2$
Threaded: $K_L = 1.5$

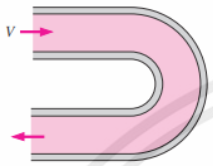

Tee (branch flow):
Flanged: $K_L = 1.0$
Threaded: $K_L = 2.0$

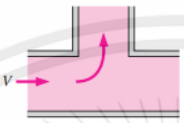

Tee (line flow):
Flanged: $K_L = 0.2$
Threaded: $K_L = 0.9$

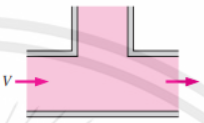

Threaded union:
$K_L = 0.08$

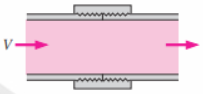

Valves

Globe valve, fully open: $K_L = 10$
Angle valve, fully open: $K_L = 5$
Ball valve, fully open: $K_L = 0.05$
Swing check valve: $K_L = 2$

Gate valve, fully open: $K_L = 0.2$
$\frac{1}{4}$ closed: $K_L = 0.3$
$\frac{1}{2}$ closed: $K_L = 2.1$
$\frac{3}{4}$ closed: $K_L = 17$

* These are representative values for loss coefficients. Actual values strongly depend on the design and manufacture of the components and may differ from the given values considerably (especially for valves). Actual manufacturer's data should be used in the final design.

Figure 3.15 Loss coefficient K_L of various pipe components for turbulent flow.

3.7 Pump [13]

A pump's function is to impart energy to a fluid, leading to a rise in fluid pressure rather than a guaranteed increase in the fluid's velocity throughout the pump.

3.7.1 Type of pump [14]

1. Dynamic

-Centrifugal: We chose this pump type because it converts rotational kinetic energy, typically from an engine or motor, into fluid flow. They comprise an impeller on a shaft within a casing, with the shaft extending through a stuffing box for fluid containment. Used across industries for fluid transportation, these pumps are valued for their simple design, ease of operation, and capacity to handle large volumes, including fluids with suspended solids.

-Special Effect

2. Positive Displacement

-Reciprocating

-Rotary

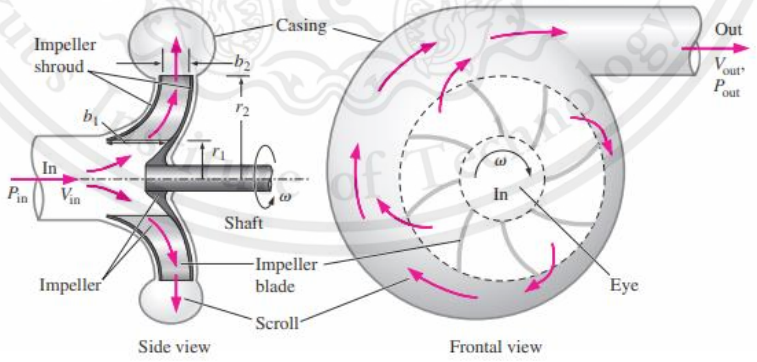

Figure 3.16 A common centrifugal pump from the side view and front view. [13]

3.8 Radiator [15]

A primary constraint in a cooling system's heat transfer occurs when heat moves from the radiator to the air. The process of heat transfer from the water to the fins is around seven times quicker than the transfer from the fins to the air, given the same exposed surface area. The radiator needs to have the capacity to eliminate a quantity of heat energy that is roughly equivalent to the heat energy generated by the engine.

Radiators come in two basic styles:

1. Down-flow radiators

The central core is positioned vertically, while the tanks are oriented horizontally. The upper tank contains a coolant substance. The flow is facilitated by a combination of pump pressure and gravity. The radiator experiences pressurization due to the movement of air. By utilizing tubes and fins, the coolant releases heat, which is then dispersed into the surrounding air. The lower tank serves as a reservoir for the cooled fluid. Within the engine, the fluid is circulated back to the combustion chambers.

2. Cross-flow radiators

In a cross-flow radiator, the tanks are positioned on opposite sides of the central core. The coolant flows from the right side to the left side of the core. While the tanks are arranged vertically, the core itself is arranged horizontally. In a cross-flow radiator, the fluid moves horizontally from right to left through the middle section. The lower pressure side of the tank is typically utilized for the radiator cap in this type of radiator.

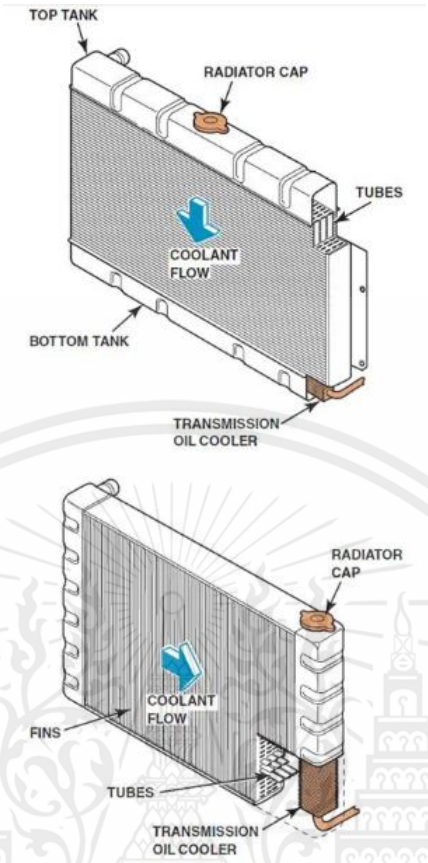

Figure 3.17 Two basic styles of radiator

Radiator Materials [17]

1. Aluminum and Plastic

Among the various kinds of car radiators, plastic and aluminum radiators consist of an aluminum core and a plastic tank.

2. Brass and Copper

Copper and brass radiators featured brass tanks and copper cores. However, plastic and aluminum radiators have replaced copper due to its high cost and susceptibility to corrosion, leading to substantial repair costs.

3. Plastic

Plastic radiators were created as a substitute for the bulky and costly copper and brass radiators. In plastic radiators, the end tanks consist of an aluminum core, while the tanks themselves are constructed from lightweight plastic material to reduce weight.

4. Aluminum

An aluminum radiator is composed of an aluminum core and tank. When compared to plastic, copper, and brass radiators, aluminum radiators exhibit noticeably superior cooling efficiency. This is primarily due to aluminum's excellent heat conduction properties, as it possesses a high thermal conductivity.

The heat transfer coefficient of both fluids that pass radiator can be calculated by.

$$
\begin{aligned}
D_h &= \frac{4A}{P} = \frac{4W+H}{2W+2H} \\
V_w &= \frac{Q_w}{N \times A} \\
Re_w &= \frac{\rho V_w D_h}{\mu_w} \\
h_w &= \frac{Nu_w \times k_w}{D_h}
\end{aligned}
\tag{3-45}
$$

$$
\begin{aligned}
V_{air} &= \frac{Q_{air}}{A_{rad} - (N_{tube} \times H_{tube} \times L_{rad})} = \frac{Q_{air}}{H_{rad} L_{rad} - (N_{tube} \times H_{tube} \times L_{rad})} \\
Re_{air} &= \frac{V_{air} W_{fin}}{V_{air}} \\
Nu_{air} &= 0.664 Re_{air}^{0.5} Pr_{air}^{1/3} \\
h_{air} &= \frac{Nu_{air} k_{air}}{W_{tube}}
\end{aligned}
\tag{3-46}
$$

Fin Dimension and efficiency

$$\eta_{fin} = \frac{\tanh(mlc)}{mlc}; m = \frac{2h_{air}}{K_{Al}H_{fin}}$$
$$L_c = L_{fin} + \frac{H_{fin}}{2} \quad (3\text{-}47)$$

Overall surface efficiency & Heat transfer coefficient

$$\eta_o = 1 - \frac{N_{fin}A_f}{A_{fin,base}}(1 - \eta_{fin})$$
$$A_f = 2W_{fin}L_c$$
$$A_b = 2L_{rad}W_{tube} - H_{fin}W_{fin}N_{fin}$$
$$A_{fin,base} = N_{fin}A_f + A_b \quad (3\text{-}48)$$
$$UA = \frac{1}{(\frac{1}{\eta_o h_{air}A_{external}}) + (\frac{1}{h_{water}A_{external}})}$$
$$A_{external} = A_{fin,base}N_{tube}$$
$$A_{internal} = (2W_{tube} + 2H_{tube})L_{rad}N_{tube}$$

Effectiveness-NTU method

$$C_{air} = \dot{m}_{air}C_{p,air}$$
$$C_{water} = \dot{m}_{water}C_{p,water} \quad (3\text{-}49)$$
$$NTU = \frac{UA}{C_{min}}$$

Heat capacity of fluid can be obtained by:

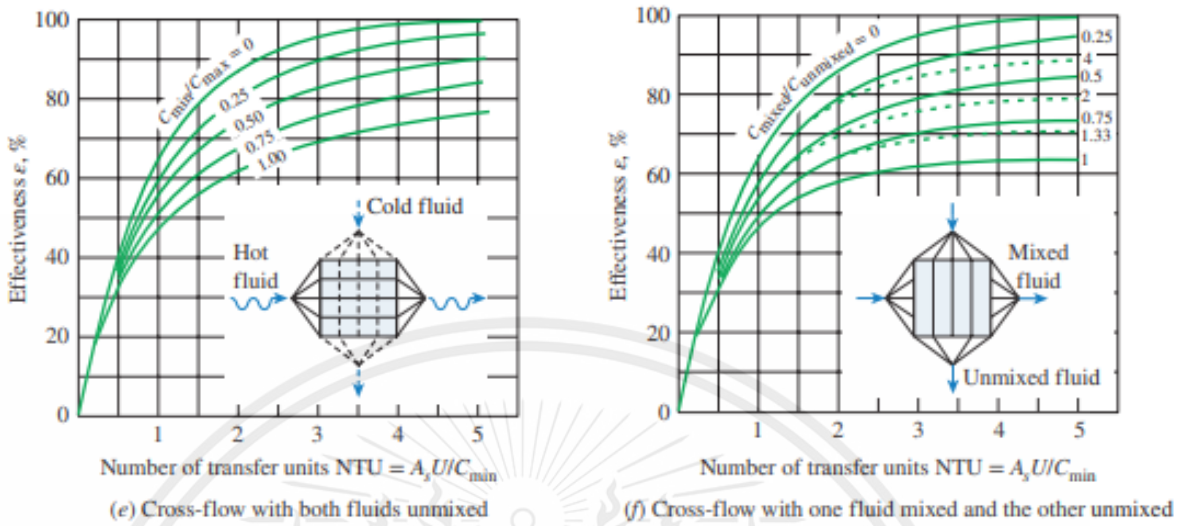

Figure 3.18 The effectiveness of cross flow heat exchanger such as radiator can be obtained.

Heat transfer rate in radiator can be calculated by.

$$q_{max} = C_{min}(T_{water,in} - T_{air,in})$$
$$q_{transfer} = \varepsilon q_{max}$$
$$T_{water,out} = T_{water,in} - \frac{q_{transfer}}{C_{water}} \quad (3\text{-}50)$$
$$T_{air,out} = T_{air,in} - \frac{q_{transfer}}{C_{air}}$$

CHAPTER 4
NUMERICAL ANALYSIS

Heat flux can significantly affect ash deposition rates in a superheater. The impact of heat flux can be understood through the processes of particle impaction, adhesion, and removal, which determine the overall ash deposition rate.

1. **Particle impaction:** As particles move with the flue gases, they can impact the superheater surfaces. The likelihood of particles sticking upon impact is influenced by the heat flux. High heat flux can lead to softening or melting of some ash particles, thus increasing their stickiness.

2. **Adhesion and building up of deposits:** Once particles adhere to the surface, they can accumulate to form an ash deposit layer. The heat flux can affect this process by altering the properties of the deposit layer. A higher heat flux might lead to sintering (where the particles join together) and a stronger deposit layer that is harder to remove.

3. **Deposit removal:** Over time, deposit layers can be removed through processes like erosion or spalling. High heat flux can lead to high thermal stresses in the deposit layer, which can cause cracks and eventually lead to removal of the deposit layer (spalling).

The proposal is to develop an equal heat flux test kit, based on the assumption that identical heat flux can induce the same rate of deposition. This test kit will enable experimental investigations into deposition rates.

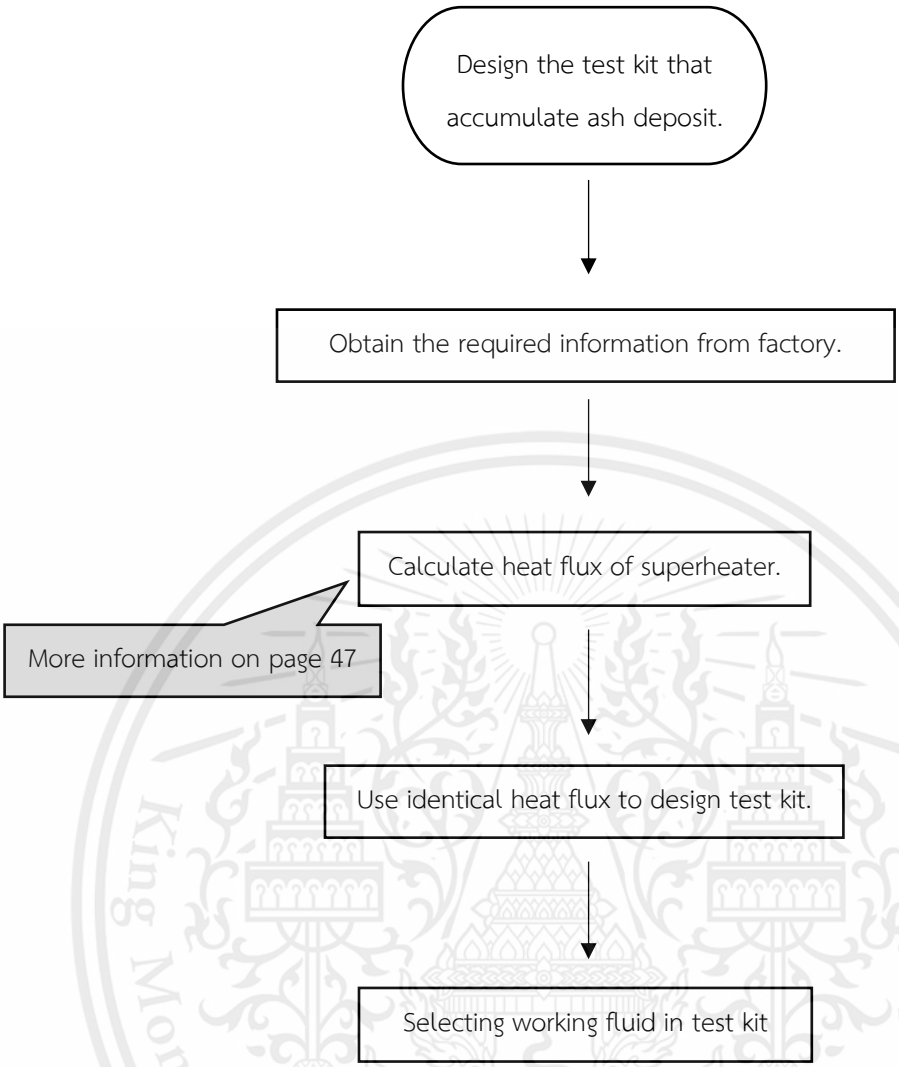

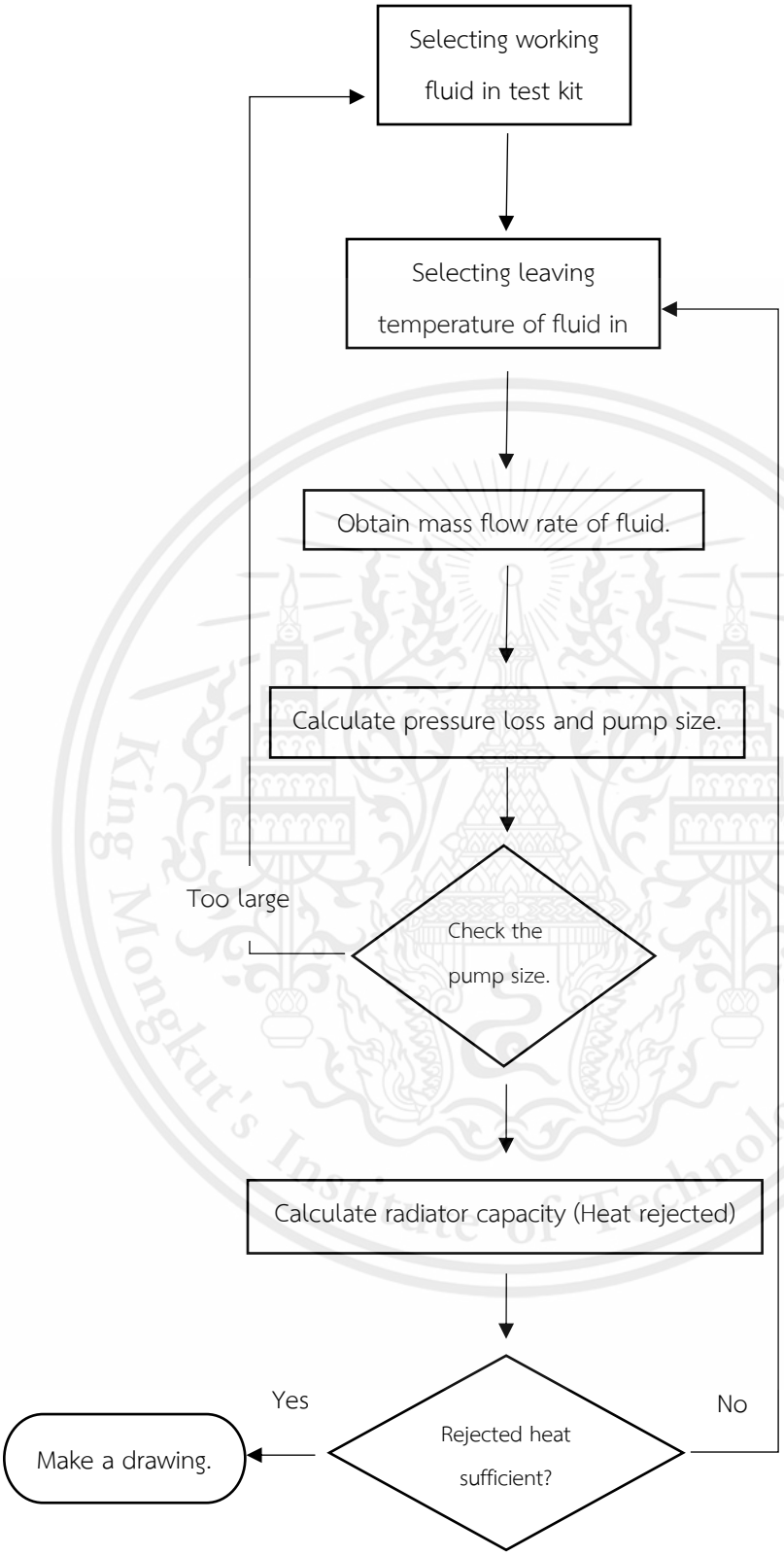

Figure 4.1 Process Flowchart

Calculate heat flux of superheater:

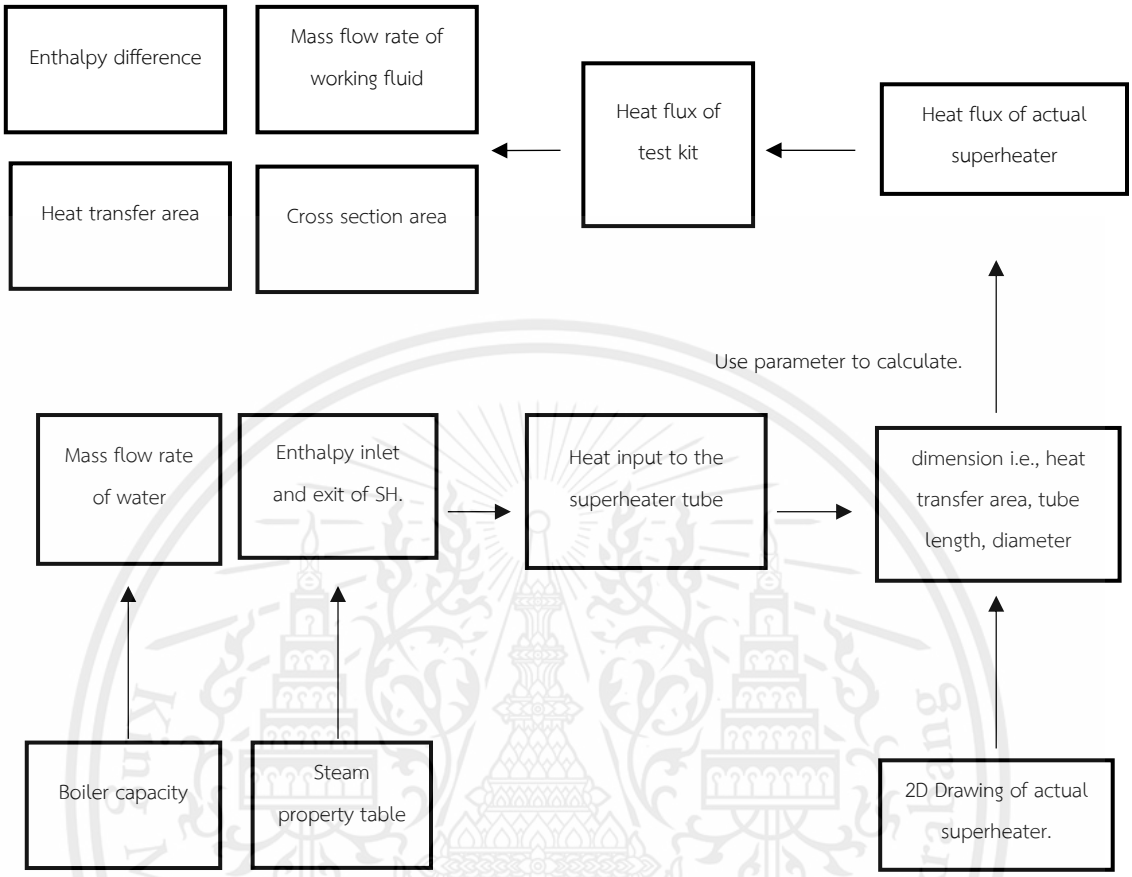

Figure 4.2 Heat flux calculation

4.1 Heat flux of superheater calculation

The heat flux of superheater can be obtained by dividing the heat turn sat vapor to superheat vapor by heat transfer area.

$$q'' = \frac{\dot{Q}_{sh}}{A} = \frac{8402.73}{285.82} = 29.3987 \text{ kw/m}^2 \quad (4\text{-}1)$$

The heat received by sat vapor can be calculated by

$$\dot{Q}_{sh} = \dot{m}_w(h_{steam} - h_{sat,vapor}) = 19.89(3223.71 - 2801.25) = 8402.73kW \quad (4\text{-}2)$$

To find $h_{sat,vapor}$ and h_{steam} the temperature or pressure must be known according to the diagram and the enthalpy can be obtain by thermodynamic property table.

Table 4.1 The properties of saturated vapor and superheat steam

Location	Phase	Pressure (kPa)	Temperature (C°)	Enthalpy (kJ/kg)
Upper drum	Saturated vapor	2351.32	220.718	2801.25
Leaving superheater	Superheated steam	2351.32	391.6	3223.71

The boiler can produce steam at 71.6 ton/hr. converted into kg/s to obtain mass flow rate of steam $\dot{m}_w$

$$\dot{m}_w = 71.6\frac{\text{ton}}{\text{hr}} \times \frac{1000\text{kg}}{1\text{ton}} \times \frac{1\text{hr}}{3600\text{s}}$$
$$\dot{m}_w = 19.89\frac{\text{kg}}{\text{s}} \quad (4\text{-}3)$$

The heat transfer area can be obtained by Fig. 4.3.

• แบบท่อน้ำเพื่อคำนวณหาพื้นที่แลกเปลี่ยนความร้อนแต่ละส่วน

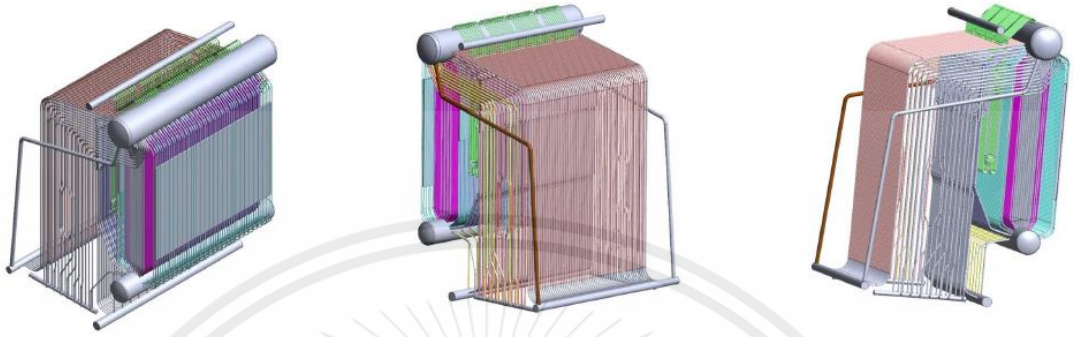

โซนที่คำนวณ	พื้นที่แลกเปลี่ยนความร้อน (m^2)
Furnace zone	537.67
Superheated zone	285.82
Back tube zone	147.92
Bank tube zone	1560.99

Figure 4.3 The heat transfer area can be obtained by the information from the factory.

4.2 Test kit calculation

Assuming the T_{in} as ambient temperature we compared air, oil and water to see the difference between C_p, $\dot{m}$, and T_{out}. By using the same heat intake as 28.1577 KW to choose which of the working fluid is suitable for the system.

Table 4.2 The comparison of the value each working fluid yields.

Working Fluid	$C_p\,(KJ/kg\cdot K)$	$\dot{m}\,(kg/s)$	$T_{out}\,(^oC)$
Air	1.02	0.6733	73
Therminol55 Oil at $32\,^oC$	2.01	0.34168	73
Water	4.18	0.1643	73

The correlation between the working fluid's mass flow rate and its exit temperature can be represented using the following mathematical expression.

$$29.3987 = \frac{\dot{m}(4.18)(T_o - 32)}{\pi(0.0508)(6)}$$
$$\frac{29.3987 \cdot \pi(0.0508)(6)}{4.18 \cdot \dot{m}} + 32 = T_o \quad (4\text{-}4)$$
$$\frac{6.7346}{\dot{m}} + 32 = T_o$$

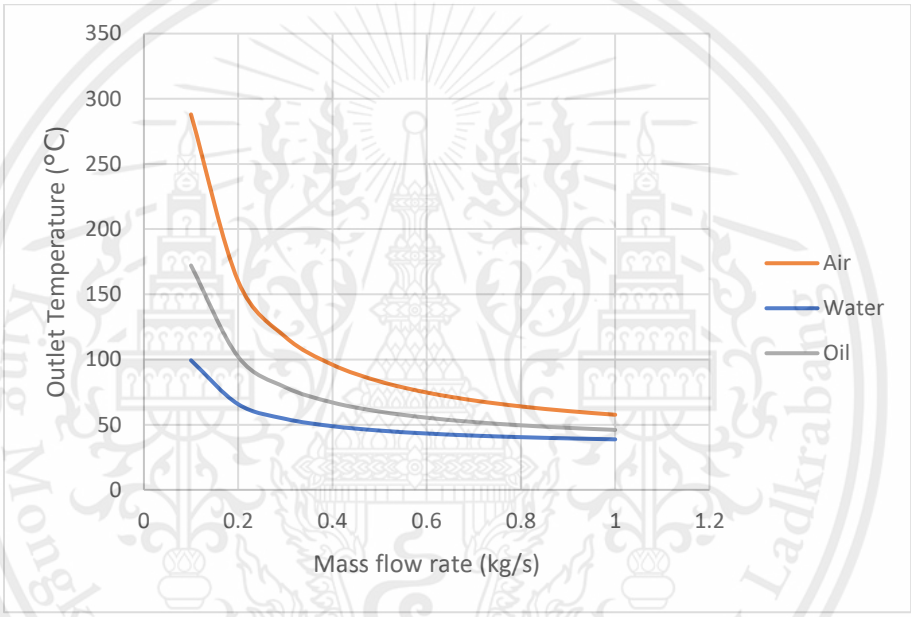

Figure 4.4 The graph of shows the different working fluids.

Reasons due to why designed outlet temperature of water is high:

1) Maintain a low mass flow rate and minimize velocity, as it is the primary factor influencing pressure loss. The increased pressure loss requires a larger pump. The greater the difference in temperature, the more effective the heat transfer in the radiator.

Calculate the heat flux of superheater.

$$q'' = \frac{\dot{Q}_{sh}}{A} = \frac{8402.73}{285.82} = 29.3987 \text{ kw/m}^2 \quad (4\text{-}5)$$

Design the test kit by mimicking heat flux of superheater.

$$29.3987 = \frac{\dot{Q}}{A} \tag{4-6}$$

Where

$$\frac{\dot{Q}}{A} = \frac{\dot{m}c_p\Delta T}{\pi D_o l} \tag{4-7}$$

Select fluid as a water so

$$29.3987 = \frac{\dot{m}(4.18)(73-32)}{\pi(0.0508)(6)}$$

$$\dot{m} = 0.1642 \text{ kg/s}$$

The heat intake of the test kit can be calculated.

$$\dot{Q} = \dot{m}_w C_p(\Delta T) = 0.1643(4.18)(73-32)$$
$$\dot{Q} = 28.1577kw \tag{4-8}$$

Obtain the relation between mass flow rate and pipe length.

$$\dot{m} = \frac{q''\pi Dl}{c_p\Delta T} = \frac{29.3987\cdot\pi Dl}{4.18(73-32)} \tag{4-9}$$

The velocity of water can be calculated as

$$\dot{m} = \rho V A_c$$
$$V = \frac{\dot{m}}{\rho A_c} \tag{4-10}$$

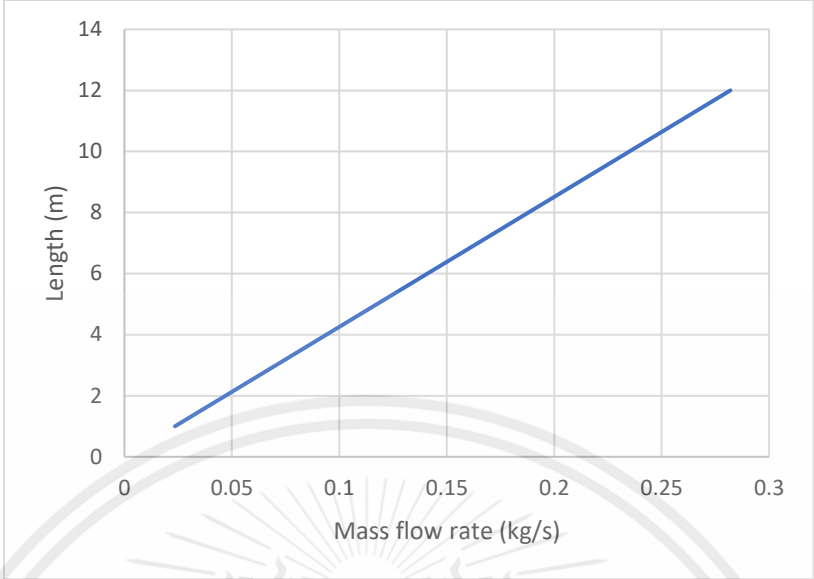

Figure 4.5 The graph can be plotted by vary the pipe length in accordance with the STBA 22 JIS G3462-1988 standard.

Table 4.3 The parameter used in calculating the pressure loss.

Parameter used in calculation	Values
Velocity (m/s)	0.2004
Gravity	9.81
Elevation, z_1 (m)	0
Elevation, z_2 (m)	0.723
Roughness, ε	0.046
Density, ρ_{water} (kg/m^3)	987.5
Inside diameter of superheater (m)	0.0428
K_L 180°	1.5
K_L 90°	0.9
K_L contract	0.6
K_L expand	0.15

The piping standard used on this test kit is JIS standard

Table 4.4 Alloy Steel Boiler and Heat Exchanger Tubes – STBA [16]

Wall Thickness (mm) / OD (mm)	50.8 mm
1.2	
1.6	
2.0	
2.3	
2.6	3.09
2.9	3.43
3.2	3.76
3.5	4.08
4.0	4.62
4.5	5.14
5.0	5.65
5.5	6.14
6.0	6.63
6.5	7.10
7.0	7.56
8.0	8.44
9.5	9.68
11.0	10.8
12.5	11.8

Table 4.5 Carbon Steel – Alloy Steel, Pipe and Tube [16]

JIS NO.		G 3452	G 3462
Grade	Current	SGP	STBA22
	Former	SGP	STBA22
Tensile Strength	Current N/mm^2	290	410
	Former Kgf/mm^2	-	42
Yield Point (Minimum)	Current N/mm^2	-	205
	Former Kgf/mm^2	-	21
Elongation*% (Minimum)	Long.	30	-
	Transv.	25	-
Rockwell Hardness (Max.) HRB		-	85

CHAPTER 5

EQUIPMENT, CONDITIONS, AND PROCEDURES

This chapter covers a full explanation of the test kit from start to end, ready for manufacturing.

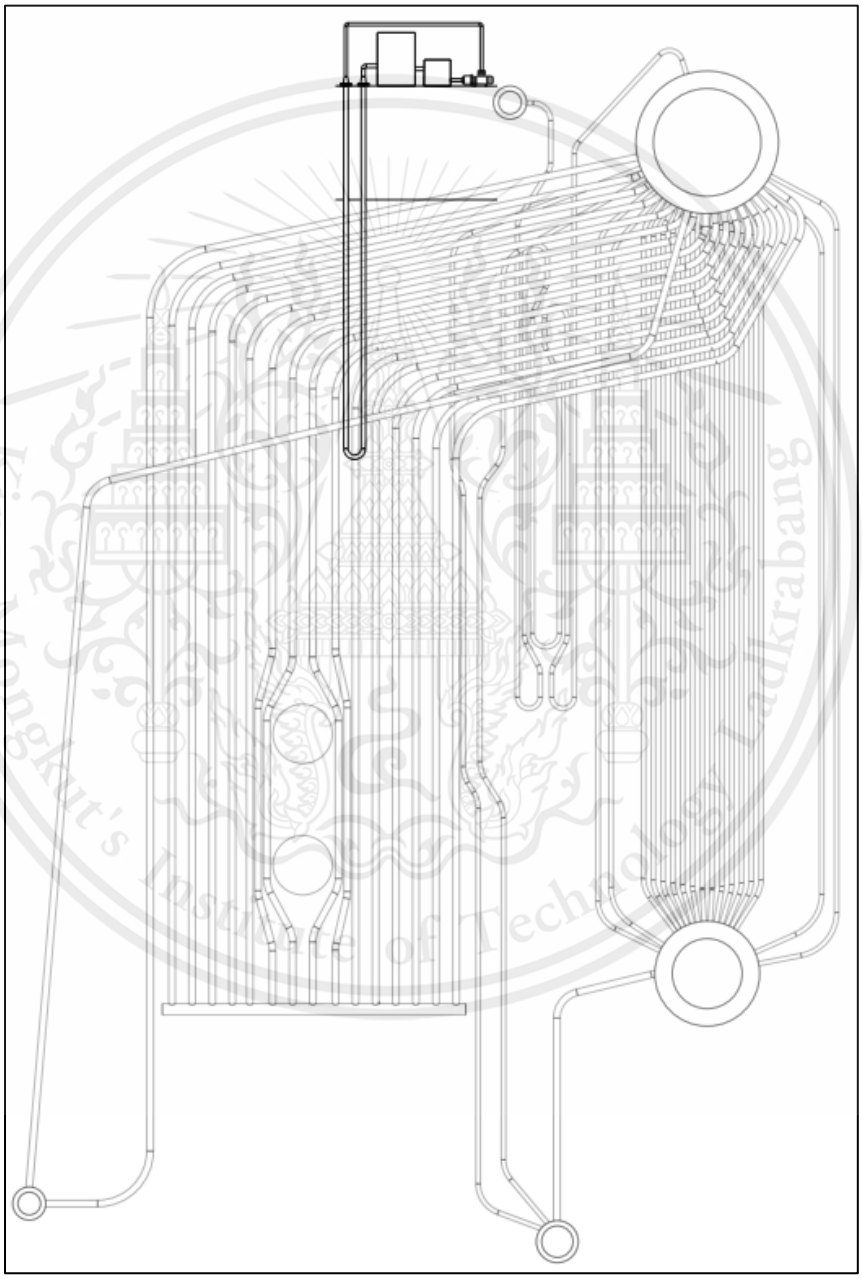

Figure 5.1 The test kit location on real plant.

Table 5.1 The operating condition of test kit.

Parameter	Values
Mass flowrate of water (kg/s)	0.1643
Velocity of water at exit point of pump (m/s)	0.2781
Velocity of water at heating section (m/s)	0.1156
Volumetric flowrate of water (m^3/s)	0.0001666
Density of water	987.5
Temperature of inlet water	32
Temperature of exit water (C)	73
Tube length (m)	6
Tube inner diameter (m)	0.0428
Tube outer diameter (m)	0.0508
Tube thickness (mm)	4
Cross section area (m^2)	0.00144
Surface area (m^2)	0.958
Reynold number	10772.3
Head loss (m)	1.6
Heat received by water (kw)	28.16

5.1 Test kit

This section will show the overview diagram of the entire system.

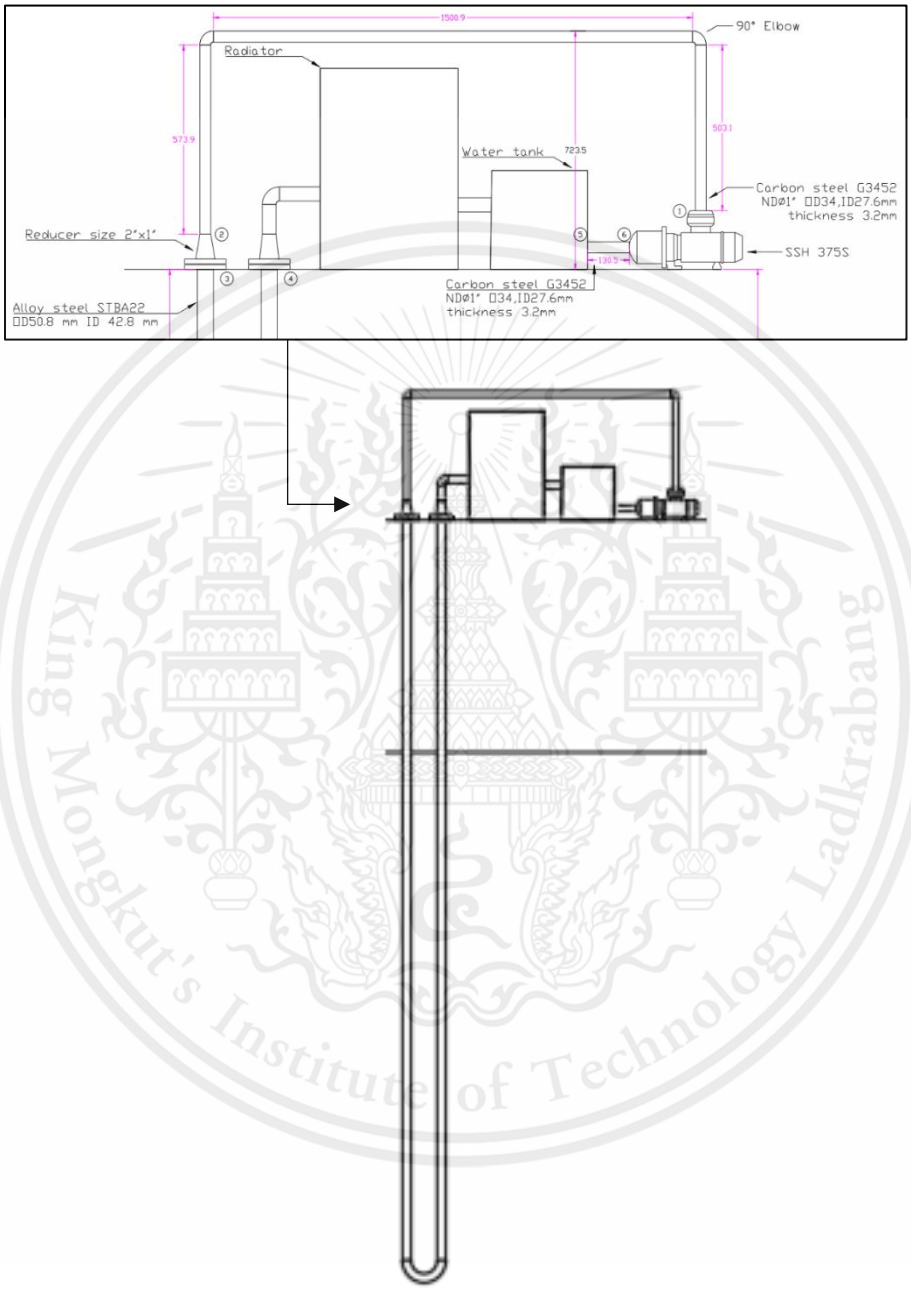

Figure 5.2 The test kit design

5.1.1 Ash deposit accumulator tube

This tube is designed to accumulate ash deposit sample to prevent the overheating of the tube the moving fluid which is water inside is take an account for receiving heat. The material of superheater is alloy steel STBA22 with the outer diameter of 50.8 mm, inner diameter of 42.8 mm, and the thickness of 4 mm.

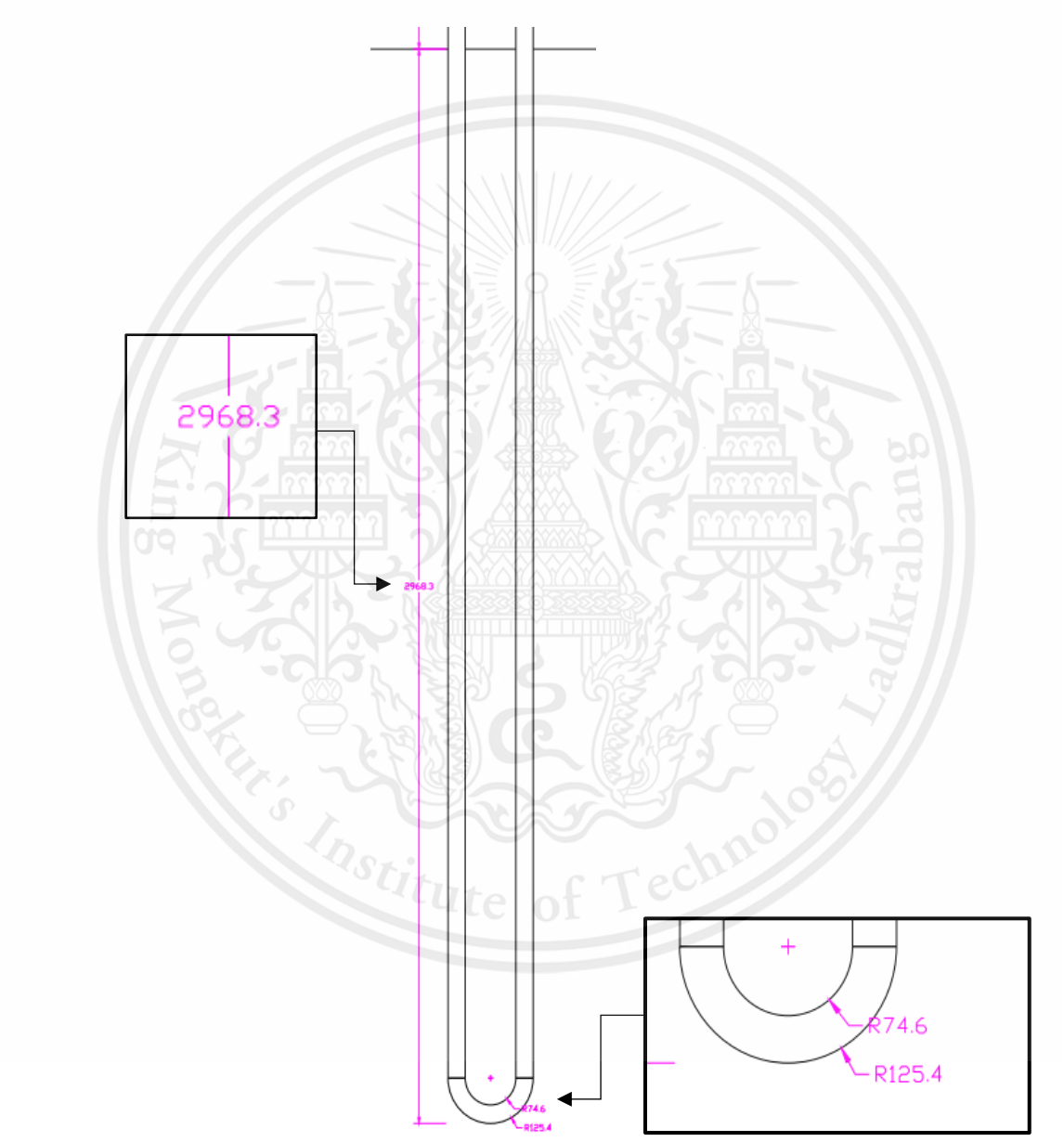

Figure 5.3 The ash deposit accumulator tube

5.1.2 Pump

Pump is equipment design to increase the energy of fluid to overcome the pressure loss both major and minor loss. After evaluating these pressure losses in terms of head, the necessary pump can be identified using the pump characteristics curve provided by the manufacturer. This will help determine if the pump can provide an adequate flow rate.

Since the calculated head loss is 1.6 m with flow rate 0.0001666 cubic meters per second (10 L/min) the SSH-375 model is consider adequate for the system.

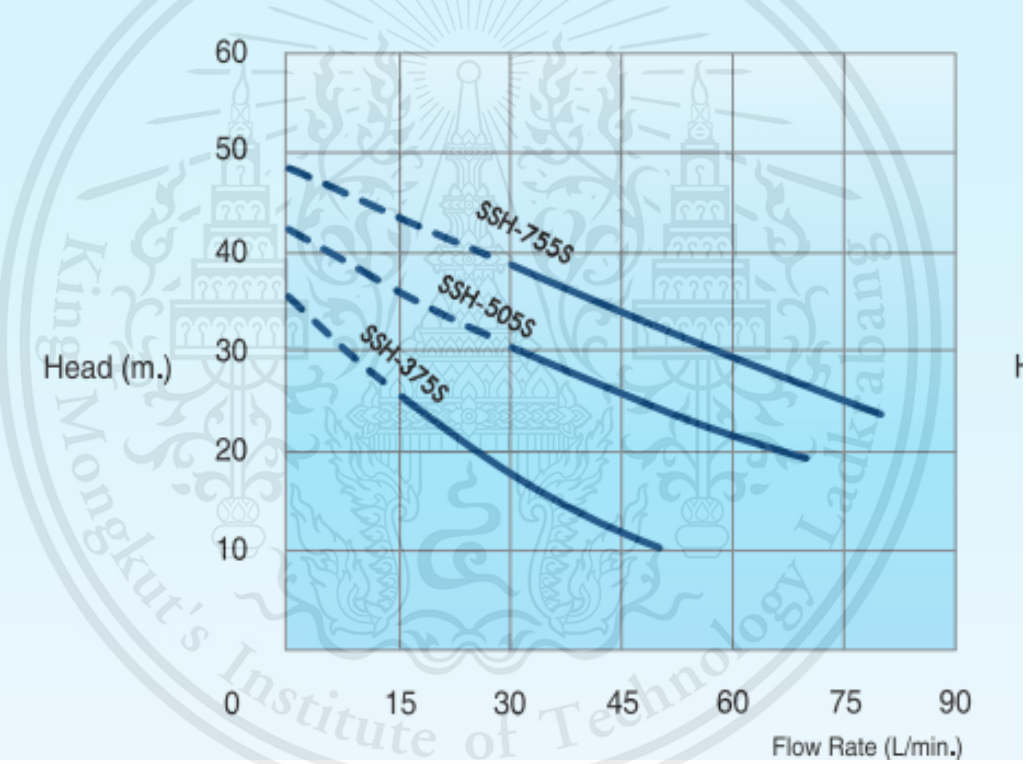

Figure 5.4 The characteristic curve of selected pump.

Dimensions

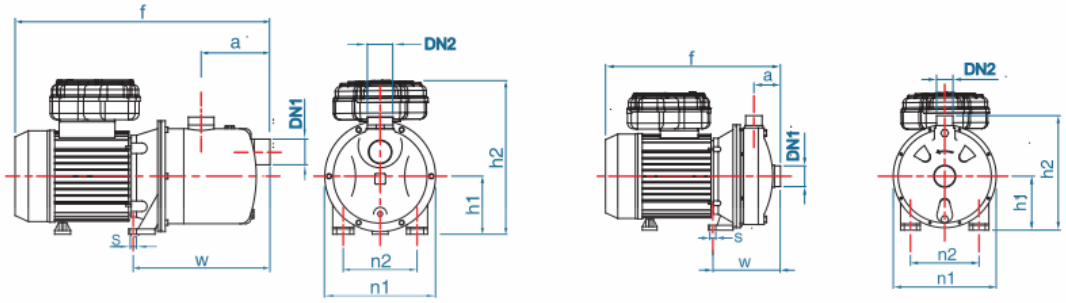

SSH-375S, SSH-505S, SSH-755S

SCM-505SH, SCM-905SH, SCM-1505SH

MODEL	BORE SIZE (Inch)		DIMENSIONS (mm.)								WEIGHT (kg.)
	DN1	DN2	a	f	h1	h2	n1	n2	w	s	
SSH-375S	1"	1"	90	354	88	178	172	100	198	9	8.5
SSH-505S	1¼"	1"	100	405	106	210	207	120	225	9	10.0
SSH-755S	1¼"	1"	100	405	106	210	207	120	225	9	12.6
SCM-505SH	1¼"	1"	49	315	110	218	213	140	138	12	9.4
SCM-905SH	1¼"	1"	49	337	110	230	213	140	138	12	15.6
SCM-1505SH	1½"	1"	49	354	110	222	213	140	138	12	21.3

Figure 5.5 Pump dimension

(https://www.meath-co.com/)

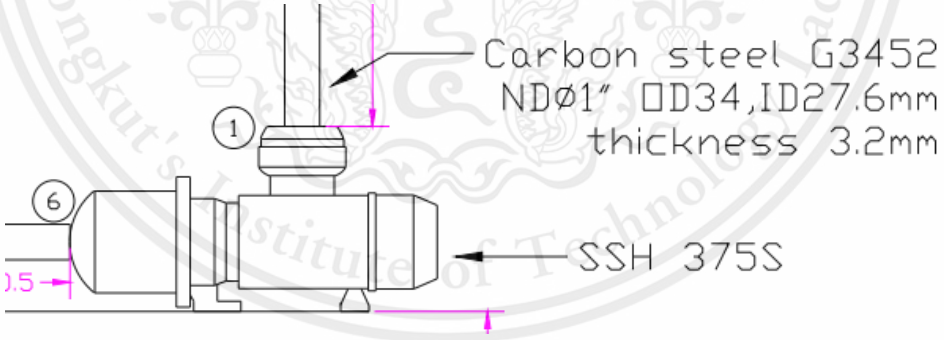

Figure 5.6 The pump design on the test kit.

5.1.3 Radiator

Radiator is used to remove the heat to decrease the temperature of water inside the tube.

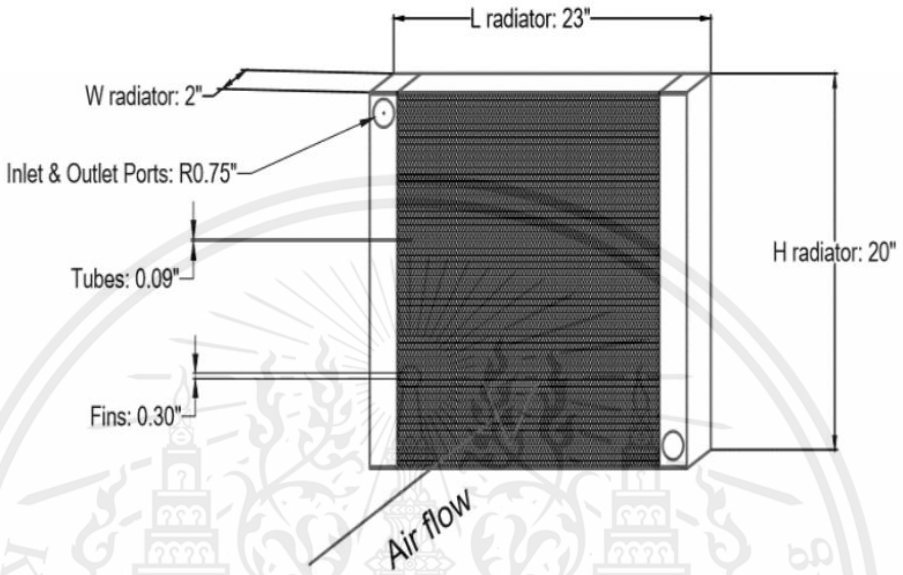

Figure 5.7 Schematic of designed radiator

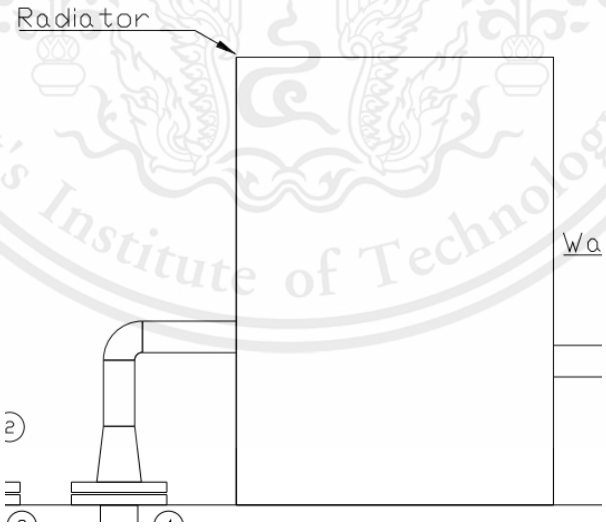

Figure 5.8 The radiator designed on the test kit.

Table 5.2 Property of selected radiator

L radiator	0.5842
H radiator	0.508
W radiator	0.0508
H tube	0.002286
W tube	0.0508
N tube	48
W fin	0.0508
L fin	0.00762
N fin	16800
H fin	0.0000254

Utilizing these parameters for computation, we ascertain that the quantity of heat (q-transfer) expelled or rejected by the radiator is quantified as 28 kilowatts.

5.1.4 Water tank

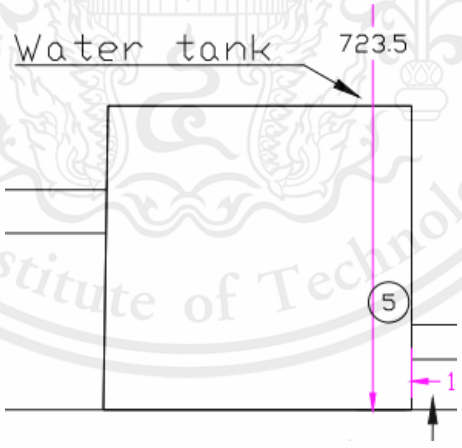

Figure 5.9 The tank design on the test kit.

The water tank in the test kit is like a water storage container. It holds the water that's used in the testing process. The water can be moved around in the system being tested.

The size of the water tank can change based on a few things:

1. System Capacity**:** The size of the system or equipment being tested will have a significant impact on the size of the water tank required. Larger systems generally require larger water tanks.

2. Test Duration**:** The length of time the test or operation is expected to run will also influence the size of the water tank. Longer tests will require more water, and thus a larger tank.

3. Flow Rate**:** The rate at which water needs to move through the system will also affect the size of the tank. Higher flow rates require a larger supply of water, necessitating a larger tank.

The design of the system includes a tank with the capability to hold up to 0.027 cubic meters of fluid, in this case, water. This is an indication of the tank's upper limit in terms of fluid volume.

A feature of the system is that it has a fluid throughput of 0.0001666 cubic meters per second. This throughput, or flow rate, represents the volume of water that is being conveyed through the system every second.

By using a simple formula of dividing the total volume by the flow rate, one can calculate the time needed to fill the tank under these conditions:

0.027 m^3 / 0.0001666 m^3/s = ~162 seconds, which is approximately 2.7 minutes.

The time required to fill the tank to capacity at the given flow rate is around 2.7 minutes. It should be noted that this is a theoretical computation and real-world factors like friction losses, pressure variations, etc., could alter the actual time required.

CHAPTER 6

CONCLUSION AND RECOMMENDATIONS

6.1 Conclusion

In this project, we developed a pilot scale design of ash deposition measurement test kit with a working fluid inside. This customized simulation model is intended to mimic ash deposit formation within a superheater. The design of the simulation employs the same heat flux value as the superheater utilized in the YOSHIMINE industrial water-tube boiler, which has a capacity of 80 tons/hour.

Several aspects must be considered when designing this test kit for accumulate ash deposition caused by combustion to occur: 1. The test tube's length must be sufficient to reach the impact point of the flue gas blowing the ash from the combustion. 2. According to the equation, the heat flux of the test kit must be close to that of the superheater $q'' = \frac{\dot{Q}}{A} = \frac{\dot{m}c_p\Delta T}{\pi Dl}$ while the heat transfer area of the test kit is proportional to the tube length.

By setting $c_p, \Delta T, D, l$ as constant values, the parameter we can change to manage the heat flux is $\dot{m}$, specifically in terms of working fluid. We discovered that when the working fluid is being used as air in an atmosphere, the pressure loss is significant, requiring the installation of a large compressor considering $\dot{m} = \rho V A_c$ at the same mass flow rate and cross section area as between water and air. We found that the density of the air is much smaller than water, which results in higher velocity. It also requires the removal of moisture from the air and c_p ($\approx 1\frac{kJ}{kg \cdot K}$) is quite low, resulting in an outlet temperature released to the atmosphere is high. As a result, to reduce costs, working fluid is water, which has a reduced pressure loss, allowing for a smaller pump with a greater c_p ($\approx 4.18\frac{kJ}{kg \cdot K}$) value and a lower outlet temperature of the water.

Another significant variable is the exit temperature of the working fluid, which in this test kit, is water. A lower exit temperature of water indicates a higher mass flow rate needed for compensation, and correspondingly, lower heat transfer as the water is cooled via the radiator. For optimizing the heat transfer rate, a larger temperature differential should be achieved. This would aid in decreasing the mass flow rate and velocity, both of which are primary factors influencing pressure loss, and subsequently, enhance the rate of heat transfer.

However, it cannot be released into the atmosphere since it must first pass through a treatment system to lower the temperature. As a result, we chose to use a radiator to cool the air to the atmosphere and not overheat the test kit. Furthermore, to avoid system malfunction, the test kit must remain in continuous operation.

For the further benefits, this test kit can be developed to measure ash deposit mass by installing a mass measurement sensor, and a thermocouple inside and outside the pipe of test kit.

6.2 Recommendations

6.2.1 Water from the supply should be pure, like reverse osmosis (RO) water. Utilizing impure water can lead to the formation of deposits within the pipe when heated, which may result in damage to the pump's impeller.

6.2.2 Prior to use, the water tank must be thoroughly cleaned to avoid debris from causing harm to the pump's impeller.

6.2.3 To extend the life of the pump, regular water assessments should be carried out.

6.2.4 To develop the appropriate test kit for a specific boiler, it is necessary to have the precise boiler dimensions in a CAD file format, which allows for accurate measurement of the required points.

6.2.5 The test kit's design is tailored to a particular piece of equipment, the YOSHIMINE industrial water-tube boiler, which has a capacity of 80 ton/hour. To adapt the test kit for use with other equipment, alterations to the design must be considered.

6.3 Further study

To determine the thickness of the ash, it is necessary to carry out the following procedure.

1. Measure the temperature of water before entering the heating section T_{in} and after T_{out} by using the temperature sensor in figure 6.2 and then calculate the heat intake by using the equation below.

$$Q(t) = \dot{m}_w C_p \left(T_{out}(t) - T_{in}(t)\right) \tag{6-1}$$

2. Find the convective gas film resistance can be found by the equation below [1].

$$R_g(t_0) = \frac{T_g(t_0) - T_{wall}(t_0)}{Q(t_0)} \tag{6-2}$$

Where T_g is the temperature of flue gas that can be measure by thermocouple which is already exist inside boiler and the T_{wall} is temperature of tube surface that can be obtain by installed the thermocouple type k in figure 6.3 with the equipment in figure 6.4.

3. Since the upstream gas velocity and temperature were relatively unchanged with time, the $R_g(t)$ can be assumed to be constant and equivalent with $R_g(t_0)$.

4. Calculate Thermal resistance R_{total} which is the combination of convective gas film resistance and the conduction resistance of deposit $R_f(t)$.

$$R_{total}(t) = \frac{T_g(t) - T_{wall}(t)}{Q(t)} \tag{6-3}$$

$$R_{total}(t) = R_g(t_0) + R_f(t) \tag{6-4}$$

By rearranging the equation, the conduction resistance due to deposit can be written as:

$$R_f(t) = R_{total}(t) - R_g(t_0)$$

$$R_f(t) = \frac{L(t)}{kA} \text{ [7]}$$

Where

$R_f(t)$ is the thermal resistance of ash deposit at time t, $(\frac{\mathrm{K}}{\mathrm{kW}})$

$L(t)$ is the thickness of ash deposit, (m)

k is the thermal conductivity of the ash, $(\frac{\mathrm{W}}{\mathrm{m}\cdot\mathrm{K}})$

A is the cross-sectional area through which the heat is flowing, (m^2)

5. The thermal conductivity of the ash can be determined through experimental methods. This involves obtaining a sample of ash and subjecting it to specific temperatures depending on whether it comes from biomass fuel (550 $^{\circ}\mathrm{C}$) or fossil fuel (750-800 $^{\circ}\mathrm{C}$). The measurement is carried out using a Heat Flow Meter (HFM). [19]

The Heat Flow Meter (HFM) consists of two plates with different temperatures: a hot plate and a cold plate. The plates are positioned with the test sample in between them. Heat is transferred from the high-temperature plate to the low-temperature plate, and the meter utilizes a sensor to measure the heat flow. When the meter reaches a steady state with a temperature gradient of zero, it calculates the thermal conductivity of the sample. The thermal conductivity of insulation materials measured using the HFM method follows standards such as ASTM C518, ISO 8301, JIS A 1412, DIN EN 13163, and others. [19]

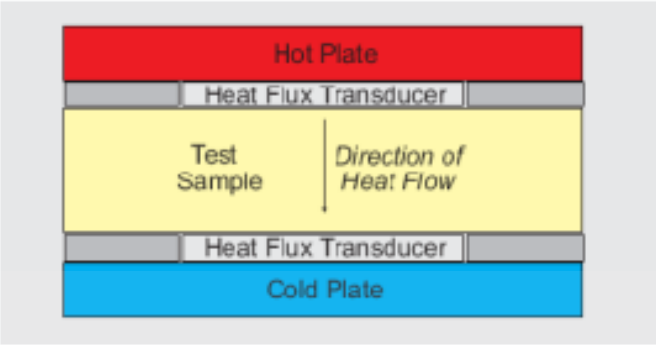

Figure 6.1 Components of Heat flow meter.

The validation of our calculation can be optain by using additional equipment below.

Figure 6.2 HANI Clamp-on Temperature Sensor

(https://landing.omega.com)

Figure 6.3 Thermocouple Type-K

(https://thai.alibaba.com)

Figure 6.4 Type K Single Input Thermometer

(https://www.nanasupplier.com)

To verify the accuracy of the selected working fluid calculation in the test kit, which in this case is water, the measurement equipment can be utilized. The flow rate can be determined using the flowmeter depicted in figures 6.5 and 6.6, while the pressure loss can be observed by referring to the pressure gauge located at the inlet and outlet, as shown in figure 6.7.

2.2 Sensor MAG 1100 FOOD

		MAG 1100 FOOD 	MAG 1100 FOOD PFA 
Type		Hygienic sensor	
Nominal size	*mm*	DN 10, 15, 25, 40, 50, 65, 80, 100	
Process connection		Hygienic adapters available for: ♦ Direct welding into dairy pipe ♦ Clamp fitting ♦ Threaded fitting	
Operating pressure		DN 10-65: 40 bar, DN 80: 37.5 bar, DN 100: 30 bar	20 bar
	Vacuum	1×10^{-6} bar	0.02 bar
Temperature of medium		–20°C to +150°C	–30°C to +130°C
		Suitable for steam sterilization	Suitable for steam sterilization at 150°C
Temperature shock		(Duration > 1 min.):	Max. ±100°C momentarily
		DN 10, 15, 25 Max. ΔT ≤ 15°C/min.	
		DN 40, 50, 65 Max. ΔT ≤ 10°C/min.	
		DN 80, 100 Max. ΔT ≤ 5°C/min.	
		(Duration ≤ 1 min., followed by 10 min. rest):	
		DN 10, 15, 25 Max. ΔT ≤ 80°C	
		DN 40, 50, 65 Max. ΔT ≤ 70°C	
		DN 80, 100 Max. ΔT ≤ 60°C	
Ambient temperature		Remote transmitter: –40°C to +100°C	Remote transmitter: –40°C to +100°C
		Compact transmitter: –20°C to +50°C	Compact transmitter: –20°C to +50°C
Liner		Aluminium oxide Al_2O_3 (ceramic)	Reinforced PFA (Teflon)
Electrodes		Platinum with gold/titanium brazing alloy	Hastelloy C-276
Enclosure		Stainless steel AISI 316 L (1.4404)	Stainless steel AISI 316 L (1.4404)
Terminal box	*Standard*	Fibre glass-reinforced polyamide	Fibre glass-reinforced polyamide
(not compact)	*Option*	Stainless steel AISI 316 (1.4436)	Stainless steel AISI 316 (1.4436)
Cable entries		4 Pg 13.5	4 Pg 13.5
Enclosure rating	*Standard*	IP 67 to EN 60529 (NEMA 4x) (1 m w.g for 30 min.)	IP 67 to EN 60529 (NEMA 4x) (1 m w.g for 30 min.)
	Option	IP 68 to EN 60529 (NEMA 6) (10 m w.g. cont.)	IP 68 to EN 60529 (NEMA 6) (10 m w.g. cont.)
Mechanical load (vibration)		18-1000 Hz random, 3.17 G rms in all directions to EN 60068-2-36	18-1000 Hz random, 3.17 G rms in all directions to EN 60068-2-36
Test pressure		80 bar (2 × PN)	40 bar (2 × PN)
Approvals		3A, EHEDG	3A
Excitation frequency		DN 10-65: 12.5 Hz	DN 10-65: 12.5 Hz
		DN 80-100: 6.25 Hz	DN 80-100: 6.25 Hz
Conforms to PED, LVT, EMC		PED - 97/23EC, LVD - 73/23 EEC + amendment 93/68/EEC, EMC - 89/336 EEX	

Figure 6.5 Siemens Electromagnetic flowmeters

(https://www.gotautomations.com)

2.5.1 Transmitter MAG 5000 (DN 2 to DN 1200)

	**Accuracy 0.5%**
Current output	
Current	0-20 mA, 4-20 mA or 4-20 mA + alarm
Load	< 800 ohm
Time constant	0.1-30 s adjustable
Digital output	
Frequency	0-10 kHz, 50% duty cycle
Time constant	0.1-30 s adjustable
Active	24 V DC, 30 mA, 1 KΩ ≤ R_{load} ≤ 10 KΩ, short-circuit-protected
Passive	3-30 V DC, max. 110 mA, 200 Ω ≤ R_{load} ≤ 10 KΩ

Figure 6.6 Transmitter for flowmeters

(https://www.gotautomations.com)

Figure 6.7 Pressure Gauge

(https://www.jksinter.com)

References

[1] T. Madhiyanon, P. Sathitruangsak, S. Sungworagarn, S. Pipatmanomai, S. Tia, “A pilot-scale investigation of ash and deposition formation during oil-palm empty-fruit-bunch (EFB) combustion” Fuel Processing Technology. 2012. Pp.250-264

[2] Anthony Lawrence Kohan, Boiler’s operator guide. McGraw-Hill. 4th Ed. 1997.

[3] กรมโรงงานอุตสาหกรรม กระทรวงอุตสาหกรรม, “โครงการถ่ายทอดเทคโนโลยีด้านความปลอดภัยแก่สถานประกอบการ: ความปลอดภัยในการใช้งานหม้อน้ำ” คู่มือการใช้งานและการดูแลรักษาหม้อน้ำ. 2553

[4] Ulrich Kleinhans, Christoph Wieland, Flemming J. Frandsen, Hartmut Spliethoff, “Ash formation and deposition in coal and biomass fired combustion systems: Progress and challenges in the field of ash particle sticking and rebound behavior” Progress in Energy and Combustion Science. 2018. Pp.65-168

[5] ฐานิตย์ เมธิยานนท์. ทฤษฎีและเทคโนโลยีการ เผาไหม้เชื้อเพลิงแข็งและชีวมวล. พิมพ์ครั้งที่ 2. กรุงเทพมหานคร : มีนเซอร์วิสซัพพลาย. 2559.

[6] Y. Cengel, M. Boles, Thermodynamics: An Engineering Approach. McGraw Hill. 8th Ed. 2015.

[7] Y. Cengel, A. Ghajar, Heat and Mass Transfer Fundamentals & Applications. McGraw Hill. 5th Ed. 2014.

[8] Japanese Industrial Standard JIS B8222:1993

[9] Yanqing Niu, Houzhang Tan, Shi’en Hui, “Ash-related issues during biomass combustion: Alkali-induced slagging, silicate melt-induced slagging (ash fusion), agglomeration, corrosion, ash utilization, and related countermeasures” Progress in Energy and Combustion Science. 2015. Pp.1-61

[10] Cai Yongtie, Yang Wenming, Zheng Zhimin, Xu Mingchen, Siah Keng Boon, Prabakaran Subbaiah, “Modelling of ash deposition in biomass boilers: a review” Energy Procedia. 2017. Pp.623–628

[11] Tae-Yong Jeong, Lkhagvadorj Sh, Jong-Ho Kim, Byoung-Hwa Lee, Chung-Hwan Jeon, “Experimental Investigation of Ash Deposit Behavior during Co-Combustion of Bituminous Coal with Wood Pellets and Empty Fruit Bunches” energies. 2019.

[12] Lei Ma, Wei Wei, Fengzhong Sun, Yuetao Shi, “Research on formation mechanism of typical low-temperature fouling layers in biomass-fired boilers” Case Studies in Thermal Engineering. 2022.

[13] Çengel, Y. A., & Cimbala, J. M., Fluid Mechanics: Fundamentals and Applications. McGraw-Hill Science/Engineering/Math. 2006.

[14] Allpumps. (2023). Classification of Pumps. All Pumps. https://allpumps.com.au/classification-of-pumps/

[15] Radiators in Automotive Engines | ASE Certification Training HQ. (n.d.). https://asecertificationtraining.com/radiators-in-automotive-engines/

[16] ประสิทธิ์ เวียงแก้วม ฉัตรชัย ลาภรังสิรัตน์. คู่มืองานท่อ Piping Quick Reference. กรุงเทพมหานคร : วี.พริ้นท์ . 2563.

[17] Jalopytalk Editorial Team. (2022). 5 Different Types of Radiators for Vehicles. Jalopy Talk. https://jalopytalk.com/types-of-radiators-for-vehicles/

[18] Paul O. Okhiria, Olumide A. Towoju. “Design and Analysis of an Automobile Radiator with a 14°C Cooling Capacity” International Journal of Scientific Research and Engineering Development-– Volume 4 Issue 5. 2021.

[19] สมจิตร พุฒดี. การวัดค่าสภาพการนำความร้อนของวัสดุ. 2021.